

# HOMOGENISATION OF A ROW OF DISLOCATION DIPOLES\*

STEPHEN JONATHAN CHAPMAN<sup>†</sup>, YANG XIANG<sup>‡</sup>, AND YICHAO ZHU<sup>‡</sup>

**Abstract.** Conventional discrete-to-continuum approaches have seen their limitation in describing the collective behaviour of the multi-polar configuration of dislocations, which are widely observed in crystalline materials. The reason is that dislocation dipoles, which play an important role in determining the mechanical properties of crystals, are smeared out when applying traditional homogenisation methods. To address such difficulties, the collective behaviour of a row of dislocation dipoles is studied by using the matched asymptotic techniques. The discrete-to-continuum transition is facilitated by introducing two field variables describing the dislocation pair density potential and the dislocation pair width. It is found by our analysis that the dislocation pair width evolves much faster than the pair density. The hierarchy in evolution time enables us to describe the dislocation dynamics by an evolution equation for the pair density coupled with an equilibrium equation for the pair width at the coarse-grained level. Such time-scale separation method may also pave a way for properly incorporating dipole-like (small but non-vanishing) dislocation structures, known as the statistically stored dislocations (SSDs) into macroscopic models of crystal plasticity in three dimensions. Moreover, the natural transition between different equilibrium patterns found here may shed light on understanding the emergence of the persistent slip bands (PSBs) in fatigue metals induced by cyclic loads.

**Key words.** dislocations, homogenisation, asymptotic analysis, persistent slip bands

**AMS subject classifications.** 74A60, 74N15, 41A60

**1. Introduction.** It is well known that the plastic deformation of crystalline materials is carried by a large number of atomistic line defects, i.e. dislocations. Hence macroscopic models of crystal plasticity can be established by formulating the dynamics of many dislocations. As an idealised (but also practically useful) case, the dynamics of straight and mutually-parallel dislocations have been intensively studied. These translationally invariant dislocations can be treated as “poles” on one of the planes perpendicular to all dislocation lines. These poles, like electrical charges, have signs depending on their line tangent with respect to the slip direction, known as the Burgers vector. Abundant experimental evidence suggests that a good understanding of the collective behaviour of many dislocation poles is important in the controlling of the mechanical properties of crystals. One example is found inside fatigued single-crystalline coppers owing to cyclic loads [13]. Before the saturation point is reached, the configuration takes a “channel-vein” structure as shown in Fig. 1(a). A vein consists of many almost straight and closely spaced edge dislocations and the veins are separated by channels where the dislocation density is relatively low. When the saturation point is reached, a characteristic “ladder”-shape structure known as the persistent slip bands (PSBs) is found forming as shown in Fig. 1(b). The walls of the ladders also consist of straight edge dislocations. The mechanism governing the transition between the channel-vein to PSB structures is still unclear and the study of the collective behaviour of edge dipoles may provide an explanation to it.

One way to reveal the role of these dislocation poles played in the formation of PSBs, is by using the two-dimensional (2D) discrete dislocation dynamical (DDD)

---

\*This work was partly supported by EPSRC through grant EP/D048400/1, and by the Hong Kong Research Grants Council through General Research Fund 606313

<sup>†</sup>Mathematical Institute, University of Oxford, Andrew Wiles Building, Radcliffe Observatory Quarter, Woodstock Road, Oxford, OX2 6GG, UK. (chapman@maths.ox.ac.uk).

<sup>‡</sup>Department of Mathematics, the Hong Kong University of Science and Technology, Clear Water Bay, Kowloon, Hong Kong, China. (maxiang@ust.hk and mayczhu@ust.hk).

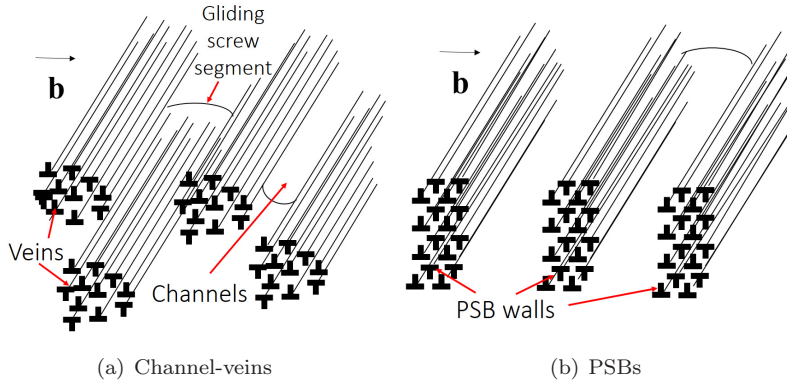


FIG. 1. Dislocation patterns in the early stage of metal fatigue induced by cyclic loads.

models, where all poles are tracked individually (e.g. [3]). Nevertheless, such DDD simulation methods not only highly rely on the computational powers, but also hardly provide any insight into the mechanism that governs the dislocation pattern formation in crystals. Hence there are still necessities of investigating the pole dynamics at the continuous level, where the dislocation substructures are described by a dislocation density distribution field. In principle, a dislocation-density-based continuum model should be obtained as the result of rigorously upscaling the 2D DDD models. However, it turns out that all existing discrete-to-continuum approaches have seen their limitation in achieving such rigorous upscaling process. The reason is as follows. At room temperature, dislocations (of edge types) are in general constrained in their own slip planes. As a result, a positive edge pole forms a pair of dipole with a nearby negative pole rather than annihilating with it, provided they do not belong to a same slip plane. Hence if applying the traditional homogenisation methods, the role of dipoles, which is crucial in determining the material mechanical properties, is completely smeared out. Owing to this, traditional homogenisation techniques are only applicable to investigate the collective behaviour of many monopoles (poles of the same sign) (e.g. [6, 14, 15]), and the collective behaviour of arbitrary multi-dislocation-pole configuration is only considered in a statistical or phenomenological manner [7, 8, 4].

To address such difficulties, the collective behaviour of a row of dislocation dipoles is rigorously studied in this paper. The discrete-to-continuum transition is facilitated by the introduction of two field variables describing the dislocation pair density potential and the dislocation pair width. By using asymptotic analysis, the dynamical relation of the row of dipoles is described by the evolutionary equations of the two field variables at the continuum level. As an outcome of the upscaling process, a transition between two discrepant dipolar patterns due to instability, which has originally discovered in periodically distributed dipoles [19], can be indicative to the reason of PSB formation.

A more general goal of this paper is to shed light on the development of dislocation-density-based continuum models in three-dimensional space, to which intensive efforts have been paid for the past two decades by many researchers (e.g. [2, 5, 10, 12]). The bottom neck is similar as what appears in the upscaling of 2D DDD models. At the continuum level, the dislocation substructures are described by a dislocation density distribution field, which is defined through the homogenisation of dislocation ensem-

bles within a small volume. However, the dislocation density field introduced in this way only takes into account the density of the geometrically necessary dislocations (GNDs). What are smeared out by the homogenisation process are the effects due to local dislocation-dislocation interactions such as dislocation line tangent effect and the statistically stored dislocations (SSDs), whose physical dimensions are smaller than the volume over which the average is taken. In three-dimensional space, the SSD structures that account for the macroscopic mechanical properties of crystals include small dislocation loops either due to source operation or thermal fluctuation, mutually locked dislocation segments like dislocation dipoles, etc. Therefore, a pivotal question to be answered for the entrenchment of a solid dislocation-density-based model is, “by what means such SSDs are incorporated into the continuum model?” Part of the question has been answered through the establishment of a continuum model of plasticity, where a set of dislocation density potential functions (DDPFs) are used to represent the dislocation substructures on a single slip plane [16, 17] and in three-dimensional space [21]. The micro-scale mechanisms that are well incorporated into the continuum model underlaid by the DDPFs are the dislocation line tangent effect [16], the grain boundary structures [18], the operation of dislocation sources of Frank-Read type [20]. The hints to the other part of the question may be found from the derived continuum model of dipole dynamics in this paper. It is shown that the time scales associated with the two field variables mentioned above are different. The dislocation pair width, which moves in response to the resolved shear stress at the leading order, varies at a time scale much faster than that associated with the dislocation pair density moving in response to the “stress gradient” (coming from the resolved shear stress at the next order). The consequence is that the fast-varying mechanism takes place so quickly that only its steady (or equilibrium) state needs to be taken into account if viewed at the slower scale. Therefore, such discrete-to-continuum approaches by asymptotically separating active processes by their associated time scales may pave a way for the incorporation of SSDs to the continuum model of plasticity characterised by DDPFs.

For these two purposes, the paper is arranged as follows. The dynamical relation of individual dislocation poles is firstly written down in § 2. After the introduction of the variables needed for the discrete-to-continuum transition, we derive for the asymptotic expression of the resolved stress field in §. 4. Then in §. 5 the equilibrium states of the row of dipoles are studied. This is followed by the derivation of the dynamical relation of the row of dipoles at the continuum level. In §. 7, the derived continuum model is validated through comparison with its underlying DDD models and further discussion is carried out in the end of the paper.

## 2. Dynamics at the level of discrete dislocations.

**2.1. Problem set up.** In this paper, we consider the case of a single slip system associated with a Burgers vector denoted by  $\mathbf{b}$  and all dislocations here are straight, mutually parallel and of edge type. The problem is thus reduced to one of the planes that are orthogonal to all dislocation tangents. Here the plane of interest is set to be the  $x$ - $y$  plane as shown in Fig. 2. Each dislocation can thus be treated as a signed pole in  $x$ - $y$  plane. In this paper, a dislocation pointing into the paper plane is set to be a positively oriented pole (termed as a “positive pole” here) and denoted by “ $\perp$ ”, while a dislocation pointing outward the paper plane is set to be a negatively oriented pole (termed as a “negative pole”) and denoted by “ $\top$ ”.

The configuration considered in this paper is as shown in Fig. 2. There are  $N + 1$  positive poles lying on the slip plane given by the  $x$ -axis, while  $N + 1$  negative poles are put within another slip plane at a distance of  $s$  from the  $x$ -axis. Here the  $n$ -th

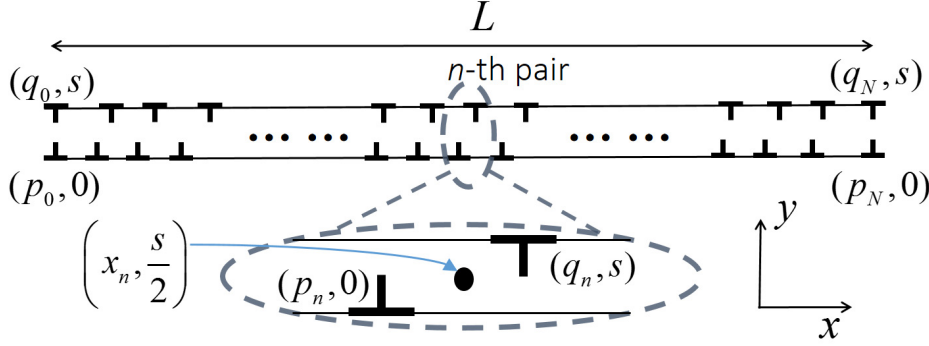


FIG. 2. The  $x$ - $y$  plane is one of the planes perpendicular to all dislocation lines. The numbers of positive and negative poles are identically  $N + 1$ . All positively oriented dislocations are located on one slip plane, which is the  $x$ -axis, and all negatively oriented poles are put on another slip plane at a distance of  $s$  from the  $x$ -axis (given by  $y = s$ ). The  $n$ -th dislocation pair consists of the  $n$ -th positive and negative poles, whose locations are set to be at  $(p_n, 0)$  and  $(q_n, s)$ , respectively. Here  $L$  is set to be the distance between the leftmost and rightmost pair centers.

dislocation pair is set to consist of the  $n$ -th positive and negative poles, which are located at  $(p_n, 0)$  and  $(q_n, s)$ , respectively.

**2.2. Dynamics.** In this paper, the motion of all dislocation poles are governed by an empirical law of motion, which is, all poles are only allowed to glide within their slip plane at a speed in proportion to their on-site resolved shear stresses. Under this rule, the motion of the  $n$ -th positive pole is given by

$$(2.1) \quad v_n^+ = \frac{dp_n}{dt} = m_g b (\tau_{\text{int}}(p_n, 0) + \tau_{\text{ext}}(p_n, 0)),$$

where  $v_n^+$  denotes the speed of the  $n$ -th positive pole along the  $x$ -axis;  $\tau_{\text{int}}(x, y)$  is the internal resolved shear stress field at  $(x, y)$  resulting from dislocation-dislocation interactions;  $\tau_{\text{ext}}(x, y)$  denotes the externally applied resolved shear stress at  $(x, y)$ ;  $m_g$  the dislocation glide coefficient;  $b = |\mathbf{b}|$ . Analogically, the gliding speed of the  $n$ -th negative pole is governed by

$$(2.2) \quad v_n^- = \frac{dq_n}{dt} = -m_g b (\tau_{\text{int}}(q_n, s) + \tau_{\text{ext}}(q_n, s)),$$

where it is worth noting that the negative sign in the right hand side of Eq. (2.2) suggests that, a positive and a negative pole move along opposite directions under a same resolved shear stress field.

Throughout this paper, we use the Greek letter  $\tau$  associated with a super- or subscript to denote resolved shear stress components due to various sources. The internal resolved shear stress field  $\tau_{\text{int}}(p_n, 0)$  is calculated by the superposition of the resolved shear stresses due to all individual poles [11]

$$(2.3) \quad \tau_{\text{int}}(p_n, 0) = \frac{\mu b}{2\pi(1-\nu)} \sum_{\substack{j=0 \\ j \neq n}}^N \frac{1}{p_n - p_j} - \frac{\mu b}{2\pi(1-\nu)} \sum_{j=0}^N \frac{(p_n - q_j)((p_n - q_j)^2 - s^2)}{((p_n - q_j)^2 + s^2)^2}.$$

Similarly, the internal resolved shear stress at  $(q_n, s)$  is calculated by

$$(2.4) \quad \tau_{\text{int}}(q_n, s) = \frac{\mu b}{2\pi(1-\nu)} \sum_{j=0}^N \frac{(q_n - p_j)((q_n - p_j)^2 - s^2)}{((q_n - p_j)^2 + s^2)^2} - \frac{\mu b}{2\pi(1-\nu)} \sum_{\substack{j=0 \\ j \neq n}}^N \frac{1}{q_n - q_j}.$$

Hence the pole dynamics at the level of discrete dislocations are given by Eq. (2.1) - (2.4), which form a closed system of ordinary differential equations with  $2(N+1)$  unknowns  $\{p_n\}_{n=0}^N$  and  $\{q_n\}_{n=0}^N$ . Then we consider reformulating the above dynamical relations at the coarse-grained level.

### 3. Set-up for discrete-to-continuum transition.

**3.1. Non-dimensionalisation.** Here it is recalled that  $L$  is the length of the domain of interest as shown in Fig. 2, we non-dimensionalise all spatial variables by  $L$ , all stress components by  $\mu Nb/(2\pi(1-\nu)L)$  and time  $t$  by  $2\pi(1-\nu)L^2/(\mu m_g Nb^2)$ . Throughout the paper, a hat is put on a variable to denote its non-dimensionalised counterpart. Hence the non-dimensionalised version of the above equation system becomes

$$(3.1) \quad \frac{d\hat{p}_n}{d\hat{t}} = \hat{\tau}_{\text{int}}(\hat{p}_n, 0) + \hat{\tau}_{\text{ext}}(\hat{p}_n, 0),$$

$$(3.2) \quad \frac{d\hat{q}_n}{d\hat{t}} = -(\hat{\tau}_{\text{int}}(\hat{q}_n, \hat{s}) + \hat{\tau}_{\text{ext}}(\hat{q}_n, \hat{s})),$$

$$(3.3) \quad \hat{\tau}_{\text{int}}(\hat{p}_n, 0) = \frac{1}{N} \sum_{\substack{j=0 \\ j \neq n}}^N \frac{1}{\hat{p}_n - \hat{p}_j} - \frac{1}{N} \sum_{j=0}^N \frac{(\hat{p}_n - \hat{q}_j)((\hat{p}_n - \hat{q}_j)^2 - \hat{s}^2)}{((\hat{p}_n - \hat{q}_j)^2 + \hat{s}^2)^2}$$

and

$$(3.4) \quad \hat{\tau}_{\text{int}}(\hat{q}_n, \hat{s}) = \frac{1}{N} \sum_{j=0}^N \frac{(\hat{q}_n - \hat{p}_j)((\hat{q}_n - \hat{p}_j)^2 - \hat{s}^2)}{((\hat{q}_n - \hat{p}_j)^2 + \hat{s}^2)^2} - \frac{1}{N} \sum_{\substack{j=0 \\ j \neq n}}^N \frac{1}{\hat{q}_n - \hat{q}_j}.$$

Here we only consider the case when the non-dimensionalised spacing between the two slip plane  $\hat{s}$  is at  $\mathcal{O}(1/N)$ , where  $\mathcal{O}$  means ‘‘the order of’’. This implies that  $\hat{s}$  can be rescaled by

$$(3.5) \quad S = \frac{\hat{s}}{N},$$

where  $S \sim \mathcal{O}(1)$ . This is because when  $\hat{s} \sim \mathcal{O}(1)$ , the slip planes are so well separated that the configuration can be treated as two rows of isolated monopoles. Such case can be studied by applying the conventional homogenisation approaches.

**3.2. Variables for discrete-to-continuum transition.** The length scale associated with Eq. (3.1) to (3.4) is characterised by the neighbouring spacings of the discrete dislocations, i.e.  $\mathcal{O}(1/N)$ . The goal of this paper is to model same dynamical relation associated with the length scale at  $\mathcal{O}(1)$ , where no isolated dislocations, but

the continuous dislocation density distribution is considered. For consistency, the expected model built at the continuum level (termed as the ‘‘continuum model’’ in this paper), should be entrenched by means of a rigorous discrete-to-continuum transition, that is, reformulating Eq. (3.1) to (3.4) by using the matched asymptotic techniques.

To facilitate such transition, we first introduce  $\hat{x}_n$  to denote the  $\hat{x}$ -coordinate of the  $n$ -th dislocation pair center, i.e.

$$(3.6) \quad \hat{x}_n = \frac{\hat{p}_n + \hat{q}_n}{2}.$$

Then a function of (non-dimensionalised) time and space denoted by  $\zeta(\hat{t}, \hat{x})$  is defined such that

$$(3.7) \quad \frac{\zeta_n}{N} := \frac{\zeta(\hat{t}, \hat{x}_n)}{N} = \hat{q}_n - \hat{p}_n,$$

where ‘‘:=’’ means ‘‘is defined to be’’, represents the width of  $n$ -th dislocation pair. Throughout the paper, a super position  $n$  put to a field variable such as  $\zeta$  indicates that the field is evaluated at  $\hat{x} = \hat{x}_n$ . Here we consider the case where the nearest negative pole of a positive one is its pair partner on its right. This limits the range of  $\zeta$  by  $\zeta \in [0, 1/2]$ .

Hence  $\hat{p}_n$  and  $\hat{q}_n$  can both be expressed in terms of  $\hat{x}_n$  and  $\zeta_n$

$$(3.8) \quad \hat{p}_n = \hat{x}_n - \frac{\zeta_n}{2N}$$

and

$$(3.9) \quad \hat{q}_n = \hat{x}_n + \frac{\zeta_n}{2N}.$$

We then introduce a dislocation density pair potential field variable  $\phi(\hat{t}, \hat{x})$ , such that

$$(3.10) \quad \phi(\hat{t}, \hat{x}_n) = \frac{n}{N} := \phi_n.$$

The function  $\phi$  here is introduced in analogy with the dislocation density potential functions defined by [16] or [21]. It can be shown that by following the argument in [16] that the dislocation pair density field denoted by  $\rho$  can be calculated by

$$(3.11) \quad \rho := \frac{\partial \phi}{\partial \hat{x}}.$$

It is worth noting that the inputs  $(\hat{t}, \hat{x})$  for all field variables appearing in the paper are omitted for simplicity. Moreover, a dash is added to a variable to denote its derivative with respect to  $\hat{x}$ . For example,

$$(3.12) \quad \phi' = \frac{\partial \phi}{\partial \hat{x}}, \quad \phi'' = \frac{\partial^2 \phi}{\partial \hat{x}^2}, \quad \dots$$

By doing that,  $\rho = \phi'$ .

Therefore, at the coarse-grained level, the dislocation substructures are described by the two field variables introduced above and the goal of this paper is to look for their governing equations through the upscaling of Eq. (3.1) - (3.4).

**4. Resolved shear stress field.** In this paper, the discrete-to-continuum transition for all quantities of interest always takes the following procedures. We start with a quantity of interest defined at the level of discrete dislocations. Then for any integer  $n \in [0, N]$ , the quantity values at  $(\hat{p}_n, 0)$  and  $(\hat{q}_n, \hat{s})$  are asymptotically expressed as functions of  $\hat{x}_n$ . Then by using the fact that  $\hat{x}_n$  is densely distributed throughout the whole domain, we can replace  $\hat{x}_n$  by  $\hat{x}$  to turn the originally obtained equations, which hold for all  $\hat{x}_n$ , to their corresponding integral-differential equations, which hold for all  $\hat{x}$ .

Following this strategy, we start by considering the asymptotic behaviour of the internal resolved shear stress field  $\hat{\tau}_{\text{int}}(\hat{p}_n, 0)$  and  $\hat{\tau}_{\text{int}}(\hat{q}_n, \hat{s})$ , given by Eq. (3.3) and (3.4), respectively. First, an interval  $\Omega_{\text{in}}^n$  is introduced associated with the  $n$ -th dislocation pair, such that the  $\hat{x}$ -coordinates of its  $2K$  neighbouring pairs of poles all fall inside  $\Omega_{\text{in}}^n$  as shown in Fig. 3. The number  $K$  here satisfies

$$(4.1) \quad 1 \ll K \ll N.$$

Throughout this paper,  $\Omega_{\text{in}}^n$  defined in this way is termed as the ‘‘inner region’’.

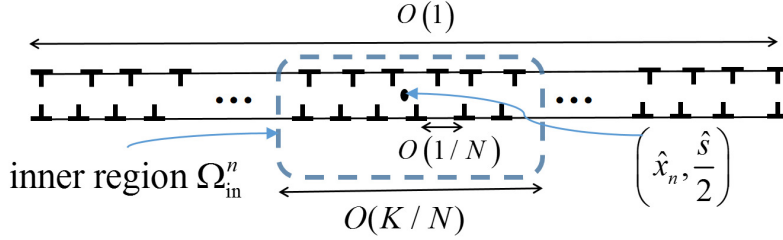


FIG. 3. Given the  $n$ -th dislocation pair, the  $\hat{x}$ -coordinates of all its  $2K$  neighbouring pairs of poles all fall inside an interval, defined to be the inner region  $\Omega_{\text{in}}^n$ , whose size is at  $\mathcal{O}(K/N)$ . Mathematically, this interval is given by Eq. (4.2). The outer region is defined to be the interval, into which the  $\hat{x}$ -coordinates of all other dislocation pair centers fall. Mathematically, it is given by Eq. (4.3).

Mathematically,  $\Omega_{\text{in}}^n$  is represented by

$$(4.2) \quad \Omega_{\text{in}}^n = \left\{ \hat{x} \left| \left| \phi(\hat{t}, \hat{x}) - \frac{n}{N} \right| \leq \frac{K}{N} \right. \right\}.$$

It can be seen that the length of  $\Omega_{\text{in}}^n$  is at  $\mathcal{O}(K/N)$ . Analogously we define an ‘‘outer region’’ by

$$(4.3) \quad \Omega_{\text{out}}^n = \left\{ \hat{x} \left| \left| \phi(\hat{t}, \hat{x}) - \frac{n}{N} \right| > \frac{K}{N} \right. \right\}.$$

Then we can estimate  $\hat{\tau}_{\text{int}}(\hat{p}_n, 0)$  in Eq. (3.3) by decomposing it into two parts

$$(4.4) \quad \hat{\tau}_{\text{int}}(\hat{p}_n, 0) = \hat{\tau}_{\text{int}}^{\text{in}}(\hat{p}_n, 0) + \hat{\tau}_{\text{int}}^{\text{out}}(\hat{p}_n, 0),$$

where  $\hat{\tau}_{\text{int}}^{\text{in}}(\hat{p}_n, 0)$  denotes the resolved shear stresses due to all poles associated with the inner region  $\Omega_{\text{in}}^n$

$$(4.5) \quad \hat{\tau}_{\text{int}}^{\text{in}}(\hat{p}_n, 0) = \sum_{\substack{j=n-K \\ j \neq n}}^{n+K} \frac{1}{\hat{p}_n - \hat{p}_j} - \sum_{j=n-K}^{n+K} \frac{(\hat{p}_n - \hat{q}_j)((\hat{p}_n - \hat{q}_j)^2 - \hat{s}^2)}{((\hat{p}_n - \hat{q}_j)^2 + \hat{s}^2)^2}$$

and  $\hat{\tau}_{\text{int}}^{\text{out}}(\hat{p}_n, 0)$  denotes all other resolved shear stress due to all poles outside  $\Omega_{\text{in}}^n$

$$(4.6) \quad \hat{\tau}_{\text{int}}^{\text{out}}(\hat{p}_n, 0) = \sum_{\substack{0 \leq j < n-K \\ n+K < j \leq N}} \left( \frac{1}{\hat{p}_n - \hat{p}_j} - \frac{(\hat{p}_n - \hat{q}_j)((\hat{p}_n - \hat{q}_j)^2 - \hat{s}^2)}{((\hat{p}_n - \hat{q}_j)^2 + \hat{s}^2)^2} \right).$$

It is worth noting that the decomposition given by Eq. (4.4) only hold for dislocations pairs that are not close to the boundaries ( $K \leq n \leq N$ ).

In a similar manner,  $\hat{\tau}(\hat{q}_n, \hat{s})$  given by Eq. (3.4) can be decomposed by

$$(4.7) \quad \hat{\tau}_{\text{int}}(\hat{q}_n, \hat{s}) = \hat{\tau}_{\text{int}}^{\text{in}}(\hat{q}_n, \hat{s}) + \hat{\tau}_{\text{int}}^{\text{out}}(\hat{q}_n, \hat{s}),$$

where

$$(4.8) \quad \hat{\tau}_{\text{int}}^{\text{in}}(\hat{q}_n, \hat{s}) = \sum_{j=n-K}^{n+K} \frac{(\hat{q}_n - \hat{p}_j)((\hat{q}_n - \hat{p}_j)^2 - \hat{s}^2)}{((\hat{q}_n - \hat{p}_j)^2 + \hat{s}^2)^2} - \sum_{\substack{j=n-K \\ j \neq n}}^{n+K} \frac{1}{\hat{q}_n - \hat{q}_j}$$

and

$$(4.9) \quad \hat{\tau}_{\text{int}}^{\text{out}}(\hat{q}_n, \hat{s}) = \sum_{\substack{0 \leq j < n-K \\ n+K < j \leq N}} \left( \frac{(\hat{q}_n - \hat{p}_j)((\hat{q}_n - \hat{p}_j)^2 - \hat{s}^2)}{((\hat{q}_n - \hat{p}_j)^2 + \hat{s}^2)^2} - \frac{1}{\hat{q}_n - \hat{q}_j} \right).$$

**4.1. Inner region approximation.** We here first look for asymptotic expressions of the resolve shear stress field  $\hat{\tau}_{\text{int}}^{\text{in}}(\hat{p}_n, 0)$ . The calculation begins with quantifying the contribution to  $\hat{\tau}_{\text{int}}^{\text{in}}(\hat{p}_n, 0)$  from the  $j$ -th positive and negative poles. Given any  $j$  so that  $\hat{x}_j$  belongs to the inner region, we consider the asymptotic expression of  $\hat{p}_j$  and  $\hat{q}_j$  near  $\hat{x}_n$ . This is found to take two steps: relating  $\hat{p}_j$  and  $\hat{q}_j$  to  $\hat{x}_j$  first and then relating  $\hat{x}_j$  to  $\hat{x}_n$ . The first step can be achieved according to Eq. (3.8) and (3.9). For the second step, we re-write Eq. (3.10) by

$$(4.10) \quad \phi(\hat{t}, \hat{x}_j) = \frac{j}{N} = \frac{n}{N} + \frac{j-n}{N} = \phi(\hat{t}, \hat{x}_n) + \frac{j-n}{N}.$$

Since in the inner region  $|\frac{j-n}{N}| \leq \frac{K}{N} \ll 1$ , one can obtain the asymptotic expansion of  $\hat{x}_j$  in terms of  $\frac{j-n}{N}$  near  $\hat{x}_n$  as

$$(4.11) \quad \hat{x}_j \sim \hat{x}_n + \frac{j-n}{N} \cdot \frac{1}{\phi'_n} - \frac{(j-n)^2}{N^2} \cdot \frac{\phi''_n}{2(\phi'_n)^3} + \frac{(j-n)^3}{N^3} \cdot \frac{(3(\phi''_n)^2 - \phi'_n \phi'''_n)}{6(\phi'_n)^5} + \mathcal{O}\left(\frac{K^4}{N^4}\right).$$

It is worth to be reminded that an index  $n$  put to  $\phi$  or  $\zeta$  suggests the evaluation is made at  $\hat{x}_n$

$$(4.12) \quad \phi'_n := \phi'(\hat{t}, \hat{x}_n), \quad \zeta_n := \zeta(\hat{t}, \hat{x}_n)$$

and so on. With Eq. (4.11), we obtain the expansion of  $\zeta_j$  near  $\zeta_n$  in terms of  $(j-n)/N$  by

$$(4.13) \quad \zeta_j = \zeta(\hat{x}_j) \sim \zeta_n + \frac{1}{N} \cdot \frac{(j-n)\zeta'_n}{\phi'_n} + \frac{1}{N^2} \cdot \frac{(j-n)^2(\zeta''_n \phi'_n - \phi''_n \zeta'_n)}{2(\phi'_n)^3} + \mathcal{O}\left(\frac{K^3}{N^3}\right).$$

It is worth noting that  $\zeta$  here should also be expanded as

$$(4.14) \quad \zeta \sim \zeta^{(0)} + \frac{\zeta^{(1)}}{N} + \dots$$

But for simplicity, we will temporarily keep  $\zeta$  unexpanded unless needed.

Hence combining Eq. (3.8), (4.11) and (4.13), we can asymptotically express  $\hat{p}_j$  near  $\hat{x}_n$  by

$$(4.15) \quad \begin{aligned} \hat{p}_j \sim \hat{x}_n &+ \frac{1}{N} \cdot \left( \frac{j-n}{\phi'_n} - \frac{\zeta_n}{2} \right) - \frac{1}{2N^2} \cdot \left( \frac{(j-n)\zeta'_n}{\phi'_n} + \frac{(j-n)^2\phi''_n}{(\phi'_n)^3} \right) \\ &+ \frac{1}{N^3} \cdot \left( \frac{(j-n)^2\zeta'_n\phi''_n}{4(\phi'_n)^3} + \frac{(j-n)^3\phi''_n}{2(\phi'_n)^5} + \frac{(j-n)^2\zeta''_n}{4(\phi'_n)^2} - \frac{(j-n)^3\phi'''_n}{6(\phi'_n)^4} \right) + \mathcal{O}\left(\frac{K^4}{N^4}\right). \end{aligned}$$

Similarly we have

$$(4.16) \quad \begin{aligned} \hat{q}_j \sim \hat{x}_n &+ \frac{1}{N} \cdot \left( \frac{j-n}{\phi'_n} + \frac{\zeta_n}{2} \right) + \frac{1}{2N^2} \cdot \left( \frac{(j-n)\zeta'_n}{\phi'_n} - \frac{(j-n)^2\phi''_n}{(\phi'_n)^3} \right) \\ &- \frac{1}{N^3} \cdot \left( \frac{(j-n)^2\zeta'_n\phi''_n}{4(\phi'_n)^3} - \frac{(j-n)^3\phi''_n}{2(\phi'_n)^5} - \frac{(j-n)^2\zeta''_n}{4(\phi'_n)^2} + \frac{(j-n)^3\phi'''_n}{6(\phi'_n)^4} \right) + \mathcal{O}\left(\frac{K^4}{N^4}\right). \end{aligned}$$

Thus we can estimate  $1/(N(\hat{p}_n - \hat{p}_j))$  appearing in Eq. (4.5) by

$$(4.17) \quad \begin{aligned} \frac{1}{N} \frac{1}{\hat{p}_n - \hat{p}_j} &\sim -\frac{\phi'_n}{j-n} - \frac{1}{N} \cdot \left( \frac{\zeta'_n}{2(j-n)} + \frac{\phi''_n}{2\phi'_n} \right) + \frac{j-n}{N^2} \cdot \left( \frac{(\phi''_n)^2}{4(\phi'_n)^3} - \frac{\phi'''_n}{6(\phi'_n)^2} \right) \\ &- \frac{1}{4N^2} \cdot \left( \frac{\phi'_n(\zeta'_n)^2}{4(j-n)} + \frac{\zeta'_n\phi''_n}{\phi'_n} + \zeta''_n \right) + \mathcal{O}\left(\frac{K^2}{N^3}\right). \end{aligned}$$

It is worth noting that when making truncation to the above expansions, the order of magnitude of  $(j-n)$  may grow as large as  $K$ . This is the reason that the terms truncated in the expansion in Eq. (4.17) is at  $\mathcal{O}(K^2/N^3)$ . Besides, it has been found as a posteriori that the internal resolved shear stresses accounting for the pair density evolution come from the next order of the expansion, which is  $\mathcal{O}(1/N)$ . Hence to ensure that the accuracy of the expansion in Eq. (4.17) meets this requirement, we further set

$$(4.18) \quad K \sim \sqrt{N}.$$

In this section unless specified, the expansions to all resolved shear stresses will be truncated at  $o(1/N)$ , where  $o$  means ‘‘smaller than the order of’’.

With reference to Eq. (4.17), the first sum in Eq. (4.5) becomes

$$(4.19) \quad \frac{1}{N} \sum_{\substack{j=n-K \\ j \neq n}}^{n+K} \frac{1}{\hat{p}_n - \hat{p}_j} \sim -\frac{K}{N} \cdot \frac{\phi''_n}{\phi'_n} + \mathcal{O}\left(\frac{K^3}{N^3}\right).$$

Analogically, to prepare for evaluating the second sum in Eq. (3.3), we have

$$(4.20) \quad \frac{(\hat{p}_n - \hat{q}_j)((\hat{p}_n - \hat{q}_j)^2 - \hat{s}^2)}{((\hat{p}_n - \hat{q}_j)^2 + \hat{s}^2)^2} \sim -\frac{\phi'_n \cdot (j - n + \phi'_n \zeta_n) \left( (j - n + \phi'_n \zeta_n)^2 - (S\phi'_n)^2 \right)}{\left( (j - n + \phi'_n \zeta_n)^2 + (S\phi'_n)^2 \right)^2}$$

$$- \frac{\phi''_n}{N\phi'_n} \cdot \frac{(j - n)^2 (j - n + \phi'_n \zeta_n)^4 - 6(j - n + \phi'_n \zeta_n)^2 (S\phi'_n)^2 + (S\phi'_n)^4}{\left( (j - n + \phi'_n \zeta_n)^2 + (S\phi'_n)^2 \right)^3}$$

$$+ \frac{1}{N^2} \cdot \frac{(j - n + \phi'_n \zeta_n)^5 (j - n)^4 (\phi''_n)^2}{\left( (j - n + \phi'_n \zeta_n)^2 + (S\phi'_n)^2 \right)^4 (\phi'_n)^3}$$

$$- \frac{1}{N^2} \cdot \frac{(j - n + \phi'_n \zeta_n)^6 (j - n)^3 (3(\phi''_n)^2 - \phi'''_n \phi'_n)}{6 \left( (j - n + \phi'_n \zeta_n)^2 + (S\phi'_n)^2 \right)^4 (\phi'_n)^3} + \mathcal{O} \left( \frac{K^2}{N^3}, \frac{1}{N^2} \right),$$

where  $\hat{s} = S/N$  defined by Eq. (3.5) is used. It is worth noting that the expansion (4.20) only holds for the case where at least one of  $S$  and  $\zeta_n$  is not too small. Otherwise the expansion in Eq. (4.20) gets singular for  $j = n$ .

Thus adding the right hand side of Eq. (4.20) over  $j$  from  $n - K$  to  $n + K$  gives rise to the asymptotic expression of the second sum in Eq. (4.5)

$$(4.21) \quad \frac{1}{N} \sum_{j=-n-K}^{n+K} \frac{(\hat{p}_n - \hat{q}_j)((\hat{p}_n - \hat{q}_j)^2 - \hat{s}^2)}{((\hat{p}_n - \hat{q}_j)^2 + \hat{s}^2)^2} \sim (\pi\phi'_n) \cdot G_0(2\pi\zeta_n\phi'_n, 2\pi S\phi'_n) + \frac{2\zeta_n\phi'_n}{K} + \frac{K\phi''_n}{N\phi'_n}$$

$$- \frac{N(\zeta_n\phi'_n)}{K^2} - \frac{\phi''_n}{N\phi'_n} \cdot G_{11}(2\pi\zeta_n\phi'_n, 2\pi S\phi'_n) - \frac{(\zeta_n\phi'_n)'}{N} \cdot G_{12}(2\pi\zeta_n\phi'_n, 2\pi S\phi'_n)$$

$$- \frac{\phi''_n\zeta'_n}{N} \cdot G_{13}(2\pi\zeta_n\phi'_n, 2\pi S\phi'_n) + o \left( \frac{1}{N} \right),$$

where

$$(4.22) \quad G_0(\alpha, \beta) = \frac{\sin \alpha}{\cosh \beta - \cos \alpha} - \frac{\beta \sin \alpha \sinh \beta}{(\cos \alpha - \cosh \beta)^2},$$

(4.23)

$$G_{11}(\alpha, \beta) = -\frac{1}{2} - \frac{\alpha \cos \alpha + 2\beta \sinh \beta}{2(\cos \alpha - \cosh \beta)} + \frac{5\beta^2(1 - \cos \alpha \cosh \beta)}{4(\cos \alpha - \cosh \beta)^2} - \frac{3\alpha\beta \sin \alpha \sinh \beta}{2(\cos \alpha - \cosh \beta)^2}$$

$$+ \frac{\beta^3 \sinh \beta (1 - \cos \alpha \cosh \beta + \sin^2 \alpha)}{4(\cos \alpha - \cosh \beta)^3} + \frac{\alpha\beta^2 \sin \alpha (1 - \cos \alpha \cosh \beta - \sinh^2 \beta)}{2(\cos \alpha - \cosh \beta)^3},$$

$$(4.24) \quad G_{12}(\alpha, \beta) = -\frac{\pi\alpha(1 - \cos \alpha \cosh \beta)}{2(\cos \alpha - \cosh \beta)^2} - \frac{\pi\alpha\beta \sinh \beta (1 - \cos \alpha \cosh \beta + \sin^2 \alpha)}{2(\cos \alpha - \cosh \beta)^3}.$$

and

$$(4.25) \quad G_{13}(\alpha, \beta) =$$

$$- \frac{\pi \sin \alpha}{2} \left( \frac{1}{\cos \alpha - \cosh \beta} + \frac{3\beta \sinh \beta}{(\cos \alpha - \cosh \beta)^2} - \frac{\beta^2(1 - \cos \alpha \cosh \beta - \sinh^2 \beta)}{(\cos \alpha - \cosh \beta)^3} \right).$$

It is noted that for above calculation, the properties of the Poly-Gamma functions (for details, see [1]) are used.

Hence we obtain the asymptotic expansion to  $\hat{\tau}_{\text{int}}^{\text{in}}(\hat{p}_n, 0)$  by incorporating Eq. (4.19) and (4.21) into (4.5), which is

$$(4.26) \quad \begin{aligned} \hat{\tau}_{\text{int}}^{\text{in}}(\hat{p}_n, 0) &\sim (\pi\phi'_n) \cdot G_0(2\pi\zeta_n\phi'_n, 2\pi S\phi'_n) + \frac{2\zeta_n\phi'_n}{K} - \frac{\zeta_n\phi'_n}{K^2} \\ &\quad - \frac{\phi''_n}{N\phi'_n} \cdot G_{11}(2\pi\zeta_n\phi'_n, 2\pi S\phi'_n) - \frac{(\zeta_n\phi'_n)'}{N} \cdot G_{12}(2\pi\zeta_n\phi'_n, 2\pi S\phi'_n) \\ &\quad - \frac{\phi'_n\zeta'_n}{N} \cdot G_{13}(2\pi\zeta_n\phi'_n, 2\pi S\phi'_n) + o\left(\frac{1}{N}\right). \end{aligned}$$

Analogously,  $\hat{\tau}_{\text{int}}^{\text{in}}(\hat{q}_n, \hat{s})$  is asymptotically calculated by

$$(4.27) \quad \begin{aligned} \hat{\tau}_{\text{int}}^{\text{in}}(\hat{q}_n, \hat{s}) &\sim (\pi\phi'_n) \cdot G_0(2\pi\zeta_n\phi'_n, 2\pi S\phi'_n) + \frac{2\zeta_n\phi'_n}{K} - \frac{\zeta_n\phi'_n}{K^2} \\ &\quad + \frac{\phi''_n}{N\phi'_n} \cdot G_{11}(2\pi\zeta_n\phi'_n, 2\pi S\phi'_n) + \frac{(\zeta_n\phi'_n)'}{N} \cdot G_{12}(2\pi\zeta_n\phi'_n, 2\pi S\phi'_n) \\ &\quad + \frac{\phi'_n\zeta'_n}{N} \cdot G_{13}(2\pi\zeta_n\phi'_n, 2\pi S\phi'_n) + o\left(\frac{1}{N}\right). \end{aligned}$$

**4.2. Outer region approximation.** For  $\hat{x}_j$  belonging to the outer region, according to Eq. (4.3), we have

$$(4.28) \quad \frac{K}{N} < |\phi(\hat{x}_n) - \phi(\hat{x}_j)| = \phi'(c_0)|\hat{x}_n - \hat{x}_j|,$$

where  $c_0$  takes some value between  $\hat{x}_j$  and  $\hat{x}_n$ . Eq. (4.28) suggests that

$$(4.29) \quad |\hat{x}_j - \hat{x}_n| \gg 1/N,$$

for all  $\hat{x}_j \in \Omega_{\text{out}}^n$ . For outer region approximation, we consider the resolved shear stress field at  $(\hat{p}_n, 0)$  due to the  $j$ -th dislocation pair, which is given according to Eq. (4.9) by

$$(4.30) \quad \frac{1}{N} \cdot \left( \frac{1}{\hat{p}_n - \hat{p}_j} - \frac{(\hat{p}_n - \hat{q}_j)((\hat{p}_n - \hat{q}_j)^2 - (S/N)^2)}{((\hat{p}_n - \hat{q}_j)^2 + (S/N)^2)^2} \right),$$

where  $\hat{s} = S/N$  is used. It is recalled from Eq. (3.8) and (3.9) that  $\hat{p}_j$  and  $\hat{q}_j$  are both away from  $\hat{x}_j$  only within a distance at  $\mathcal{O}(1/N)$  and so are  $\hat{p}_n$  and  $\hat{q}_n$  from  $\hat{x}_n$ . Thus combining Eq. (4.29), we have

$$(4.31) \quad |\hat{p}_n - \hat{p}_j| \sim |\hat{p}_n - \hat{q}_j| \sim |\hat{x}_n - \hat{x}_j| \gg \frac{1}{N}.$$

Then one may combine Eq. (3.8) and (3.9) to obtain the expansion of Eq. (4.30) as

$$(4.32) \quad \begin{aligned} \frac{1}{N} \cdot \left( \frac{1}{\hat{p}_n - \hat{p}_j} - \frac{(\hat{p}_n - \hat{q}_j)((\hat{p}_n - \hat{q}_j)^2 - (S/N)^2)}{((\hat{p}_n - \hat{q}_j)^2 + (S/N)^2)^2} \right) &\sim -\frac{1}{N^2} \cdot \frac{\zeta_j}{(\hat{x}_n - \hat{x}_j)^2} \\ &\quad + \frac{1}{N^3} \cdot \frac{\zeta_n\zeta_j - 3S^2}{(\hat{x}_n - \hat{x}_j)^3} + \frac{1}{N^4} \cdot \frac{3\zeta_j(6S^2 - \zeta_n^2) + 18S^2\zeta_n - \zeta_j}{4(\hat{x}_j - \hat{x}_n)^4} + \mathcal{O}\left(\frac{1}{K^5}\right). \end{aligned}$$

It is implied from Eq. (4.32) that the leading order effect of the stress at  $(\hat{p}_n, 0)$  due to the positive pole at  $(\hat{p}_j, 0)$  cancels with that due to its pair partner located at  $(\hat{q}_n, \hat{s})$ .

Here two points are worth being addressed. Firstly, when the truncation is made,  $1/|\hat{x}_j - \hat{x}_n|$  can be as large as  $\mathcal{O}(N/K)$ . Secondly, the summation made for outer region approximation involves almost  $N$  terms. This means that to ensure an accuracy of  $o(1/N)$  for a quantity resulting from a summation over almost  $N$  terms, the truncation made at each term in the summation should be at  $o(1/N^2)$ . Hence a truncation at  $\mathcal{O}(1/K^5)$  is made in Eq. (4.32), where  $K \sim \sqrt{N}$ .

Based on Eq. (4.32), the expansion for  $\hat{\tau}_{\text{int}}^{\text{out}}(\hat{p}_n, 0)$  defined in Eq. (4.6) is obtained

$$(4.33) \quad \begin{aligned} \hat{\tau}_{\text{int}}^{\text{out}}(\hat{x}_n, 0) \sim & -\frac{1}{N^2} \cdot \sum_{\substack{0 \leq j < n-K \\ n+K < j \leq N}} \frac{\zeta_j}{(\hat{x}_n - \hat{x}_j)^2} + \frac{1}{N^3} \cdot \sum_{\substack{0 \leq j < n-K \\ n+K < j \leq N}} \frac{\zeta_n \zeta_j - 3S^2}{(\hat{x}_n - \hat{x}_j)^3} \\ & + \frac{1}{N^4} \cdot \sum_{\substack{0 \leq j < n-K \\ n+K < j \leq N}} \frac{3\zeta_j(6S^2 - \zeta_n^2) + 18S^2\zeta_n - \zeta_j}{4(\hat{x}_j - \hat{x}_n)^4} + \mathcal{O}\left(\frac{N}{K^5}\right) \end{aligned}$$

To estimate the sums appearing in Eq. (4.33), one may make use of the Euler-Maclaurin formula. For example, the first sum in Eq. (4.33) over  $0 \leq j \leq n - K - 1$  can be approximated by

$$(4.34) \quad \begin{aligned} \frac{1}{N^2} \cdot \sum_{j=0}^{n-K-1} \frac{\zeta_j}{(\hat{x}_n - \hat{x}_j)^2} &= \frac{1}{N^2} \cdot \sum_{j=0}^{n-K-1} \frac{\zeta(\phi^{-1}(j/N))}{(\hat{x}_n - \phi^{-1}(j/N))^2} \\ &\sim \frac{1}{N} \int_0^{\frac{n-K-1}{N}} \frac{\zeta(\phi^{-1}(\xi)) d\xi}{(\hat{x}_n - \phi^{-1}(\xi))^2} + \frac{1}{2N^2} \left( \frac{\zeta_{n-K+1}}{(\hat{x}_n - \hat{x}_{n-K-1})^2} + \frac{\zeta_0}{(\hat{x}_n - \hat{x}_0)^2} \right) + \mathcal{O}\left(\frac{1}{K^3}\right), \end{aligned}$$

where

$$(4.35) \quad \phi^{-1}(\zeta) := \hat{x},$$

provided  $\phi(\hat{t}, \hat{x}) = \zeta$ . The integral in Eq. (4.34) can be evaluated by using integration by part

$$(4.36) \quad \begin{aligned} \int_0^{(n-K-1)/N} \frac{\zeta(\phi^{-1}(\xi)) d\xi}{(\hat{x}_n - \phi^{-1}(\xi))^2} &= \int_{\hat{x}_0}^{x_{n-K-1}} \frac{\phi'(a)\zeta(a) da}{(\hat{x}_n - t)^2} \\ &= \frac{\phi'(a)\zeta(a)}{\hat{x}_n - a} \Big|_{a=\hat{x}_0}^{a=x_{n-K-1}} - \int_{\hat{x}_0}^{x_{n-K-1}} \frac{(\phi'(a)\zeta(a))' da}{\hat{x}_n - a}, \end{aligned}$$

where  $\phi'(a)$  is the short form of  $\phi'(\hat{t}, a)$ . Hence the first sum in Eq. (4.34) over  $0 \leq j < n - K$  can be calculated by

$$(4.37) \quad \begin{aligned} -\frac{1}{N^2} \cdot \sum_{j=0}^{n-K-1} \frac{\zeta_j}{(\hat{x}_n - \hat{x}_j)^2} &= \frac{1}{N} \cdot \left( -\frac{\phi'_{n-K-1}\zeta_{n-K-1}}{\hat{x}_n - \hat{x}_{n-K-1}} + \frac{\phi'_0\zeta_0}{\hat{x}_n - x_0} \right) \\ &+ \int_{\hat{x}_0}^{x_{n-K-1}} \frac{(\phi'(a)\zeta(a))' da}{\hat{x}_n - a} - \frac{1}{2N} \cdot \frac{\zeta_{n-K+1}}{(\hat{x}_n - \hat{x}_{n-K-1})^2} + \mathcal{O}\left(\frac{1}{K^3}\right). \end{aligned}$$

The truncation stops at  $\mathcal{O}(1/K^3)$  because  $1/K^3 = 1/N^{3/2} \ll 1/N$ .

The first sum in Eq. (4.33) over  $n + K + 1 \leq j \leq N$  is calculated in analogy

$$(4.38) \quad -\frac{1}{N^2} \cdot \sum_{j=n+K+1}^N \frac{\zeta_j}{(\hat{x}_n - \hat{x}_j)^2} = \frac{\phi'_{n+K+1} \zeta_{n+K+1}}{\hat{x}_n - \hat{x}_{n+K+1}} - \frac{\phi'_N \zeta_N}{\hat{x}_n - \hat{x}_N} \\ + \int_{\hat{x}_{n+K+1}}^{\hat{x}_N} \frac{(\phi'(a)\zeta(a))' da}{\hat{x}_n - a} - \frac{1}{2N} \cdot \frac{\zeta_{n+K+1}}{(\hat{x}_n - \hat{x}_{n+K+1})^2} + \mathcal{O}\left(\frac{1}{K^3}\right).$$

Combining Eq. (4.37) and (4.38), we get the asymptotic expansion to the first sum in Eq. (4.33)

$$(4.39) \quad -\frac{1}{N^2} \cdot \sum_{\substack{0 \leq j \leq n-K \\ n+K+1 \leq j \leq N}} \frac{\zeta_j}{(\hat{x}_n - \hat{x}_j)^2} \sim \frac{1}{N} \cdot \left( \frac{\phi'_{n+K+1} \zeta_{n+K+1}}{\hat{x}_n - \hat{x}_{n+K+1}} - \frac{\phi'_N \zeta_{n-K-1}}{\hat{x}_n - \hat{x}_{n-K-1}} \right) \\ + \frac{1}{N} \cdot \left( \frac{\zeta_0}{\hat{x}_0 - \hat{x}_0} - \frac{\zeta_N}{\hat{x}_n - \hat{x}_n} \right) + \frac{1}{N} \int_{\hat{x}_0}^{\hat{x}_N} \frac{(\phi'(a)\zeta(a))' da}{\hat{x}_n - a} \\ - \frac{1}{2N^2} \cdot \left( \frac{\zeta_{n+K+1}}{(\hat{x}_n - \hat{x}_{n+K+1})^2} - \frac{\zeta_{n-K-1}}{(\hat{x}_n - \hat{x}_{n-K-1})^2} \right) + \mathcal{O}\left(\frac{1}{K^3}\right),$$

where “ $\int$ ” denotes that the integration is calculated in the following way

$$(4.40) \quad \int_{\hat{x}_0}^{\hat{x}_N} \frac{(\phi'(a)\zeta(a))' da}{\hat{x}_n - a} = \lim_{\epsilon \rightarrow 0} \left( \int_{\hat{x}_n+\epsilon}^{\hat{x}_N} \frac{(\phi'(a)\zeta(a))' da}{\hat{x}_n - a} + \int_{\hat{x}_0}^{\hat{x}_n-\epsilon} \frac{(\phi'(a)\zeta(a))' da}{\hat{x}_n - a} \right).$$

Similarly, if we define

$$(4.41) \quad g(a) = \phi'(a)(\zeta(a)\zeta_n - 3S^2),$$

we can asymptotically calculate the second sum from 0 to  $n - K - 1$  in Eq. (4.33) as

$$(4.42) \quad \frac{1}{N^3} \sum_{\substack{0 \leq j \leq n-K-1 \\ n+K+1 \leq j \leq N}} \frac{\zeta_j \zeta_n - 3S^2}{(\hat{x}_n - \hat{x}_j)^3} \\ \sim \frac{1}{2N} \frac{g(a)}{(\hat{x}_n - a)^2} \Big|_{a=\hat{x}_0}^{a=\hat{x}_{n-K-1}} - \frac{1}{N} \frac{g'(a)}{\hat{x}_n - a} \Big|_{a=\hat{x}_0}^{a=\hat{x}_{n-K-1}} \\ + \frac{1}{2N} \frac{g(a)}{(\hat{x}_n - a)^2} \Big|_{a=\hat{x}_{n-K-1}}^{a=\hat{x}_N} - \frac{1}{N} \frac{g'(a)}{\hat{x}_n - a} \Big|_{a=\hat{x}_{n-K-1}}^{a=\hat{x}_N} + \mathcal{O}\left(\frac{1}{K^3}, \frac{1}{NK}\right) \\ \sim \frac{1}{2N} \left( \frac{\phi_{n+K+1}(\zeta_{n+K+1}\zeta_n - 3S^2)}{(\hat{x}_n - \hat{x}_{n+K+1})^2} - \frac{\phi_{n-K-1}(\zeta_{n-K-1}\zeta_n - 3S^2)}{(\hat{x}_n - \hat{x}_{n-K-1})^2} \right) + o\left(\frac{1}{N}\right).$$

In a similar manner, the third sum in Eq. (4.33) is found at  $o(1/N)$ .

Therefore, incorporating Eq. (4.39) and (4.42) into (4.33), we obtain

$$(4.43) \quad \hat{\tau}_{\text{int}}^{\text{out}}(\hat{p}_n, 0) \sim \frac{\phi'_{n+K+1} \zeta_{n+K+1}}{\hat{x}_n - \hat{x}_{n+K+1}} - \frac{\phi'_{n-K-1} \zeta_{n-K-1}}{\hat{x}_n - \hat{x}_{n-K-1}} + \frac{\phi'_0 \zeta_0}{\hat{x}_n - \hat{x}_0} - \frac{\phi'_N \zeta_N}{\hat{x}_n - \hat{x}_N} \\ + \int_{\hat{x}_0}^{\hat{x}_N} \frac{(\phi'(a)\zeta(a))' da}{\hat{x}_n - a} - \frac{1}{2N} \cdot \left( \frac{\phi'_{n-K+1} \zeta_{n-K-1}}{(\hat{x}_n - \hat{x}_{n-K-1})^2} + \frac{\phi'_{n+K+1} \zeta_{n+K+1}}{(\hat{x}_n - \hat{x}_{n+K+1})^2} \right) \\ + \frac{1}{2N} \left( \frac{\phi_{n+K+1}(\zeta_{n+K+1}\zeta_n - 3S^2)}{(\hat{x}_n - \hat{x}_{n+K+1})^2} - \frac{\phi_{n-K-1}(\zeta_{n-K-1}\zeta_n - 3S^2)}{(\hat{x}_n - \hat{x}_{n-K-1})^2} \right) + o\left(\frac{1}{N}\right)$$

To further simplify the expansion of  $\hat{\tau}_{\text{int}}^{\text{out}}(\hat{p}_n, 0)$ , we employ the expansion that

$$(4.44) \quad \hat{x}_{n-K-1} \sim \hat{x}_n - \frac{K+1}{N} \cdot \frac{1}{\phi'_n} - \frac{(K+1)^2}{N^2} \cdot \frac{\phi''_n}{2(\phi'_n)^3} + \mathcal{O}\left(\frac{K^3}{N^3}\right),$$

$$(4.45) \quad \hat{x}_{n+K+1} \sim \hat{x}_n + \frac{K+1}{N} \cdot \frac{1}{\phi'_n} - \frac{(K+1)^2}{N^2} \cdot \frac{\phi''_n}{2(\phi'_n)^3} + \mathcal{O}\left(\frac{K^2}{N^2}\right),$$

$$(4.46) \quad \zeta_{n-K-1} \sim \zeta_n - \frac{K+1}{N} \cdot \frac{\zeta'_n}{\phi'_n} + \mathcal{O}\left(\frac{K^2}{N^2}\right),$$

and

$$(4.47) \quad \zeta_{n+K+1} \sim \zeta_n + \frac{K+1}{N} \cdot \frac{\zeta'_n}{\phi'_n} + \mathcal{O}\left(\frac{K^2}{N^2}\right),$$

due to the fact  $(K+1)/N \ll 1$ . Thus Eq. (4.43) can be reduced to

$$(4.48) \quad \begin{aligned} \hat{\tau}_{\text{int}}^{\text{out}}(p_n, 0) &\sim \frac{2}{K} \cdot (\zeta_n \phi'_n) - \frac{1}{K^2} \cdot \zeta_n \phi'_n + \frac{1}{N} \cdot \left( \frac{\phi'_0 \zeta_0}{\hat{x}_n - \hat{x}_0} - \frac{\phi'_N \zeta_N}{\hat{x}_n - \hat{x}_N} \right) \\ &+ \frac{1}{N} \int_{\hat{x}_0}^{\hat{x}_N} \frac{(\phi'(a)\zeta(a))' da}{\hat{x}_n - a} + o\left(\frac{1}{N}\right). \end{aligned}$$

In a similar way, we find that

$$(4.49) \quad \hat{\tau}_{\text{out}}(\hat{q}_n, \hat{s}) \sim \hat{\tau}_{\text{out}}(\hat{p}_n, 0) + o(1/N).$$

**4.3. Total resolved shear stress.** Now we combine the contributions to  $\tau_{\text{int}}(\hat{p}_n, 0)$  from both the inner and outer regions respectively formulated by Eq. (4.26) and (4.48) and we have

$$(4.50) \quad \begin{aligned} \hat{\tau}_{\text{int}}(\hat{p}_n, 0) &\sim (\pi \phi'_n) \cdot G_0(2\pi \phi_n \zeta_n, 2\pi S \phi'_n) + \frac{1}{N} \cdot \left( \frac{\phi'_0 \zeta_0}{\hat{x}_n - \hat{x}_0} - \frac{\phi'_N \zeta_N}{\hat{x}_n - \hat{x}_N} \right) \\ &+ \frac{1}{N} \int_{\hat{x}_0}^{\hat{x}_N} \frac{(\phi'(a)\zeta(a))' da}{\hat{x}_n - a} - \frac{\phi''_n}{N \phi'_n} \cdot G_{11}(2\pi \phi'_n \zeta_n, 2\pi S \phi'_n) \\ &- \frac{(\phi'_n \zeta_n)'}{N} \cdot G_{12}(2\pi \phi'_n \zeta_n, 2\pi S \phi'_n) - \frac{\phi''_n \zeta'_n}{N} \cdot G_{13}(2\pi \phi'_n \zeta_n, 2\pi S \phi'_n) + o\left(\frac{1}{N}\right). \end{aligned}$$

It is worth noting that the  $\mathcal{O}(N/K)$  and  $\mathcal{O}(N/K^2)$  terms from the inner expansion cancel with their counterparts from the outer expansion. As a result, no trace of the intermediate parameter  $K$  is seen in Eq. (4.50).

To find the asymptotic expansion for the internal resolved shear stress at  $(\hat{p}_n, 0)$ , one also needs to employ the expansion to  $\zeta$  given by Eq. (4.14). Thus with Eq. (4.50)

the full asymptotic expansion of  $\hat{\tau}_{\text{int}}(\hat{p}_n, 0)$  is given by

(4.51)

$$\begin{aligned} \hat{\tau}_{\text{int}}(\hat{p}_n, 0) &\sim (\pi\phi'_n) \cdot G_0(2\pi\phi_n\zeta_n^{(0)}, 2\pi S\phi'_n) + \frac{1}{N} \cdot \left( \frac{\phi'_0\zeta_0^{(0)}}{\hat{x}_n - \hat{x}_0} - \frac{\phi'_N\zeta_N^{(0)}}{\hat{x}_n - \hat{x}_n} \right) \\ &+ \frac{1}{N} \int_{\hat{x}_0}^{\hat{x}_n} \frac{(\phi'(a)\zeta(a)^{(0)})' dt}{\hat{x}_n - t} + \frac{\zeta_n^{(1)}}{N} \cdot \frac{\partial G_0(2\pi\phi_n\zeta_n^{(0)}, 2\pi S\phi'_n)}{\partial \zeta_n^{(0)}} \\ &- \frac{\phi_n''}{N\phi'_n} \cdot G_{11}(2\pi\phi'_n\zeta_n^{(0)}, 2\pi S\phi'_n) - \frac{(\phi'_n\zeta_n^{(0)})'}{N} \cdot G_{12}(2\pi\phi'_n\zeta_n^{(0)}, 2\pi S\phi'_n) \\ &- \frac{\phi_n''(\zeta_n^{(0)})'}{N} \cdot G_{13}(2\pi\phi'_n\zeta_n^{(0)}, 2\pi S\phi'_n) + o\left(\frac{1}{N}\right). \end{aligned}$$

Similarly, one can obtain the expansion for  $\hat{\tau}_{\text{int}}(\hat{q}_n, \hat{s})$  defined by Eq. (3.4)

(4.52)

$$\begin{aligned} \hat{\tau}_{\text{int}}(\hat{q}_n, \hat{s}) &\sim (\pi\phi'_n) \cdot G_0(2\pi\phi_n\zeta_n^{(0)}, 2\pi S\phi'_n) + \frac{1}{N} \cdot \left( \frac{\phi'_0\zeta_0^{(0)}}{\hat{x}_n - \hat{x}_0} - \frac{\phi'_N\zeta_N^{(0)}}{\hat{x}_n - \hat{x}_n} \right) \\ &+ \frac{1}{N} \int_{\hat{x}_0}^{\hat{x}_n} \frac{(\phi'(a)\zeta(a)^{(0)})' dt}{\hat{x}_n - t} + \frac{\zeta_n^{(1)}}{N} \cdot \frac{\partial G_0(2\pi\phi_n\zeta_n^{(0)}, 2\pi S\phi'_n)}{\partial \zeta_n^{(0)}} \\ &+ \frac{\phi_n''}{N\phi'_n} \cdot G_{11}(2\pi\phi'_n\zeta_n^{(0)}, 2\pi S\phi'_n) + \frac{(\phi'_n\zeta_n^{(0)})'}{N} \cdot G_{12}(2\pi\phi'_n\zeta_n^{(0)}, 2\pi S\phi'_n) \\ &+ \frac{\phi_n''(\zeta_n^{(0)})'}{N} \cdot G_{13}(2\pi\phi'_n\zeta_n^{(0)}, 2\pi S\phi'_n) + o\left(\frac{1}{N}\right). \end{aligned}$$

A comparison between Eq. (4.51) and (4.52) suggests that the leading order terms of  $\hat{\tau}_{\text{int}}(\hat{p}_n, 0)$  and  $\hat{\tau}_{\text{int}}(\hat{q}_n, \hat{s})$  are the same. At  $\mathcal{O}(1/N)$ , terms including  $G_{11}$ ,  $G_{12}$  and  $G_{13}$  are of opposite signs for  $\hat{\tau}_{\text{int}}(\hat{p}_n, 0)$  and  $\hat{\tau}_{\text{int}}(\hat{q}_n, \hat{s})$  while all other terms are identical. Hence one may express  $\hat{\tau}_{\text{int}}(\hat{p}_n, 0)$  and  $\hat{\tau}_{\text{int}}(\hat{q}_n, \hat{s})$  in a simpler way that

$$(4.53) \quad \hat{\tau}_{\text{int}}(\hat{p}_n, 0) \sim \tau_{\text{int}}^{(0)}(\hat{x}_n) + \frac{\hat{\tau}_{\text{same}}^{(1)}(\hat{x}_n) - \hat{\tau}_{\text{opp}}^{(1)}(\hat{x}_n)}{N} + o\left(\frac{1}{N}\right)$$

and

$$(4.54) \quad \hat{\tau}_{\text{int}}(\hat{q}_n, \hat{s}) \sim \tau_{\text{int}}^{(0)}(\hat{x}_n) + \frac{\hat{\tau}_{\text{same}}^{(1)}(\hat{x}_n) + \hat{\tau}_{\text{opp}}^{(1)}(\hat{x}_n)}{N} + o\left(\frac{1}{N}\right),$$

respectively, where

$$(4.55) \quad \hat{\tau}_{\text{int}}^{(0)}(\hat{x}_n) = (\pi\phi'_n) \cdot G_0(2\pi\phi_n\zeta_n^{(0)}, 2\pi S\phi'_n),$$

$$(4.56) \quad \begin{aligned} \hat{\tau}_{\text{same}}^{(1)}(\hat{x}_n) &= \frac{\phi'_0\zeta_0^{(0)}}{\hat{x}_n - \hat{x}_0} - \frac{\phi'_N\zeta_N^{(0)}}{\hat{x}_n - \hat{x}_n} + \int_{\hat{x}_0}^{\hat{x}_N} \frac{(\phi'(a)\zeta^{(0)}(a))' da}{\hat{x}_n - a} \\ &+ \zeta_n^{(1)} \cdot \frac{\partial G_0(2\pi\phi_n\zeta_n^{(0)}, 2\pi S\phi'_n)}{\partial \zeta_n^{(0)}} \end{aligned}$$

and

$$(4.57) \quad \hat{\tau}_{\text{opp}}^{(1)}(\hat{x}_n) = \frac{\phi_n''}{\phi_n'} \cdot G_{11}(2\pi\phi_n'\zeta_n^{(0)}, 2\pi S\phi_n') + (\phi_n'\zeta_n^{(0)})' \cdot G_{12}(2\pi\phi_n'\zeta_n^{(0)}, 2\pi S\phi_n') \\ + (\zeta_n^{(0)})'\phi_n'' \cdot G_{13}(2\pi\phi_n'\zeta_n^{(0)}, 2\pi S\phi_n').$$

Accordingly the external stress  $\hat{\tau}_{\text{ext}}$  at  $(\hat{p}_n, 0)$  is also expanded near  $(\hat{x}_n, 0)$

$$(4.58) \quad \hat{\tau}_{\text{ext}}(\hat{p}_n, 0) \sim \hat{\tau}_{\text{ext}}^0(\hat{x}_n) - \frac{\zeta_n^{(0)}}{2N} \cdot \frac{\partial \hat{\tau}_{\text{ext}}^0(\hat{x}_n)}{\partial \hat{x}} + o\left(\frac{1}{N}\right),$$

where for simplicity

$$(4.59) \quad \hat{\tau}_{\text{ext}}^0(\hat{x}_n) := \hat{\tau}_{\text{ext}}(\hat{x}_n, 0), \quad \frac{\partial \hat{\tau}_{\text{ext}}^0(\hat{x}_n)}{\partial \hat{x}} = \frac{\partial \hat{\tau}_{\text{ext}}}{\partial \hat{x}} \Big|_{(\hat{x}_n, 0)}.$$

Similarly,

$$(4.60) \quad \hat{\tau}_{\text{ext}}(\hat{q}_n, \hat{s}) \sim \hat{\tau}_{\text{ext}}^0(\hat{x}_n) + \frac{1}{N} \left( \frac{\zeta_n^{(0)}}{2} \cdot \frac{\partial \hat{\tau}_{\text{ext}}^0(\hat{x}_n)}{\partial \hat{x}} + S \cdot \frac{\partial \hat{\tau}_{\text{ext}}^0(\hat{x}_n)}{\partial \hat{y}} \right) + o\left(\frac{1}{N}\right),$$

where

$$(4.61) \quad \frac{\partial \hat{\tau}_{\text{ext}}^0(\hat{x}_n)}{\partial \hat{y}} = \frac{\partial \hat{\tau}_{\text{ext}}}{\partial \hat{y}} \Big|_{(\hat{x}_n, 0)}.$$

Therefore, the total resolved shear stress at  $(\hat{p}_n, 0)$  is expressed by

$$(4.62) \quad \hat{\tau}_{\text{tot}}(\hat{p}_n, 0) \sim \hat{\tau}_{\text{int}}^{(0)}(\hat{x}_n) + \hat{\tau}_{\text{ext}}^0(\hat{x}_n) + \frac{1}{N} \left( \hat{\tau}_{\text{same}}^{(1)}(\hat{x}_n) - \hat{\tau}_{\text{opp}}^{(1)}(\hat{x}_n) + \frac{\zeta_n^{(0)}}{2} \frac{\partial \hat{\tau}_{\text{ext}}^0(\hat{x}_n)}{\partial \hat{x}} \right) + o\left(\frac{1}{N}\right).$$

Similarly,

$$(4.63) \quad \hat{\tau}_{\text{tot}}(\hat{q}_n, \hat{s}) \sim \hat{\tau}_{\text{int}}^{(0)}(\hat{x}_n) + \hat{\tau}_{\text{ext}}^0(\hat{x}_n) + \frac{\hat{\tau}_{\text{same}}^{(1)}(\hat{x}_n) + \hat{\tau}_{\text{opp}}^{(1)}(\hat{x}_n)}{N} \\ + \frac{\zeta_n^{(0)}}{2N} \cdot \frac{\partial \hat{\tau}_{\text{ext}}^0(\hat{x}_n)}{\partial \hat{x}} + \frac{S}{N} \cdot \frac{\partial \hat{\tau}_{\text{ext}}^0(\hat{x}_n)}{\partial \hat{y}} + o\left(\frac{1}{N}\right).$$

## 5. Equilibria.

**5.1. Force balance equations.** With the asymptotic results of the resolved shear stress at each pole derived, we now consider the case when the system reaches its equilibrium state. In this scenario, the total resolved shear stress  $\hat{\tau}_{\text{tot}}(\hat{p}_n, 0)$  and  $\hat{\tau}_{\text{tot}}(\hat{q}_n, \hat{s})$  should be zero for all  $n$  according to the law of motion governed by Eq. (3.1) and (3.2). By letting the right hand side of Eq. (4.62) and (4.63) vanish, we asymptotically obtain one equation (associated with  $n$ ) from the leading order,  $\mathcal{O}(1)$ ,

$$(5.1) \quad \hat{\tau}_{\text{int}}^{(0)}(\hat{x}_n) + \hat{\tau}_{\text{ext}}^0(\hat{x}_n) = 0$$

and two equations (associated with  $n$ ) from the next order,  $\mathcal{O}(1/N)$ ,

$$(5.2) \quad \hat{\tau}_{\text{same}}^{(1)}(\hat{x}_n) - \hat{\tau}_{\text{opp}}^{(1)}(\hat{x}_n) - \frac{\zeta_n^{(0)}}{2} \cdot \frac{\partial \hat{\tau}_{\text{ext}}^0(\hat{x}_n)}{\partial \hat{x}} = 0;$$

$$(5.3) \quad \hat{\tau}_{\text{same}}^{(1)}(\hat{x}_n) + \hat{\tau}_{\text{opp}}^{(1)}(\hat{x}_n) + \frac{\zeta_n^{(0)}}{2} \cdot \frac{\partial \hat{\tau}_{\text{ext}}^0(\hat{x}_n)}{\partial \hat{x}} + S \cdot \frac{\partial \hat{\tau}_{\text{ext}}^0(\hat{x}_n)}{\partial \hat{y}} = 0.$$

There are  $3(N+1)$  unknowns  $\{\phi'_n\}_{n=0}^N$ ,  $\{\zeta_n^{(0)}\}_{n=0}^N$  and  $\{\zeta^{(1)}\}_{n=0}^N$  contained in the above equations. But it is worth noting that we are interested in the leading order term of  $\zeta_n$ , which is  $\zeta_n^{(0)}$ . Since it can be checked that  $\zeta_n^{(1)}$  only appears in  $\hat{\tau}_{\text{same}}^{(1)}(\hat{x}_n)$ , one may subtract Eq. (5.3) by (5.2) to eliminate  $\zeta_n^{(1)}$  and obtain

$$(5.4) \quad 2\hat{\tau}_{\text{opp}}^{(1)}(\hat{x}_n) + \zeta_n^{(0)} \cdot \frac{\partial \hat{\tau}_{\text{ext}}^0(\hat{x}_n)}{\partial \hat{x}} + S \cdot \frac{\partial \hat{\tau}_{\text{ext}}^0(\hat{x}_n)}{\partial \hat{y}} = 0.$$

Thus Eq. (5.1) and (5.4) form a set of equations with  $2(N+1)$  unknowns  $\{\phi'_n\}_{n=0}^N$  and  $\{\zeta_n^{(0)}\}_{n=0}^N$  to determine. Here we simply drop the superscript “(0)” from  $\zeta^{(0)}$  by only considering the leading-order effect.

Since  $\hat{x}_n$  is densely distributed in the domain, we may drop the index  $n$  to re-write Eq. (5.1) and (5.4) as two coupling differential equations for  $\phi'$  and  $\zeta$ :

$$(5.5) \quad \hat{\tau}_{\text{int}}^{(0)} + \hat{\tau}_{\text{ext}}^0 = 0$$

and

$$(5.6) \quad 2\hat{\tau}_{\text{opp}}^{(1)} + \zeta \cdot \frac{\partial \hat{\tau}_{\text{ext}}^0}{\partial \hat{x}} + S \cdot \frac{\partial \hat{\tau}_{\text{ext}}^0}{\partial \hat{y}} = 0.$$

## 5.2. Equilibria under almost zero externally applied stress.

**5.2.1. Possible equilibrium states and their stability.** Since the situation is still complicated to analyse Eq. (5.5) and (5.6), we start with a simple case where the externally applied resolved shear stress almost vanishes, i.e.

$$(5.7) \quad \hat{\tau}_{\text{ext}}^0 = 0.$$

Then with reference to Eq. (4.55) and (4.57), Eq. (5.5) and (5.6) become

$$(5.8) \quad G_0(2\pi\zeta\phi', 2\pi S\phi') = 0$$

and

$$(5.9) \quad 0 = \frac{2\phi''}{\phi'} \cdot G_{11}(2\pi\phi'\zeta, 2\pi S\phi') + 2(\phi'\zeta)' \cdot G_{12}(2\pi\phi'\zeta, 2\pi S\phi') \\ + 2(\phi'(\zeta)') \cdot G_{13}(2\pi\phi'\zeta, 2\pi S\phi') + \zeta \frac{\partial \hat{\tau}_{\text{ext}}^0}{\partial \hat{x}} + S \frac{\partial \hat{\tau}_{\text{ext}}^0}{\partial \hat{y}}.$$

With reference to the expression for  $G_0$  in Eq. (4.22), Eq. (5.8) becomes

$$(5.10) \quad \frac{\sin(2\pi\phi'\zeta)}{\cosh(2\pi S\phi') - \cos(2\pi\phi'\zeta)} \cdot \left( 1 - \frac{2\pi S\phi' \sinh(2\pi S\phi')}{\cosh(2\pi S\phi') - \cos(2\pi\phi'\zeta)} \right) = 0.$$

Eq. (5.10) can be regarded as an implicit relation between two quantities  $\phi'\zeta$  and  $\phi'S$ . In fact, these two quantities are physically meaningful. Since the pair density  $\phi'$  is approximately the reciprocal of the spacing between two neighbouring pair centers

scaled by  $N$ ,  $\phi'S$  is effectively the ratio of slip plane gap to the pair center spacing. Also  $\phi'\zeta$  measures how the pair width is compared with the pair center spacing. Actually, it is observed that if we set  $X = \phi'\zeta$  and  $Y = \phi'S$ , we go back to the same setting-up used for the study of periodic dipoles [19].

From Eq. (5.10), there are three possible solutions for  $\zeta$  in terms of  $\phi'$  and other parameters.

- Equilibrium Type I when  $\zeta = 0$ . Within each dislocation pair, the positive and the negative poles are vertically aligned as shown in Fig. 4(a).
- Equilibrium Type II when  $\phi'\zeta = 1/2$ . Since  $\phi'\zeta$  represents the ratio of pair width to pair center spacing, we conclude that every negative pole lies roughly in the middle of two neighbouring positive poles as shown in Fig. 4(b) for Equilibrium Type II.
- Equilibrium Type III when

$$(5.11) \quad \zeta = \frac{1}{2\pi\phi'} \cos^{-1} (\cosh(2\pi S\phi') - 2\pi S\phi' \sinh(2\pi S\phi')).$$

In contrast to Equilibrium Type II, a positive pole here is combined with a negative one to form a localised structure, that is, a real dipole as shown in Fig 4(c).

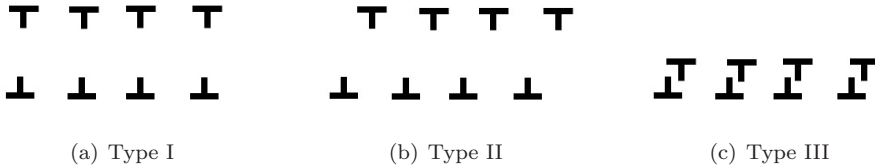


FIG. 4. *Three types of equilibria: (a)  $\zeta = 0$ ; (b)  $\zeta\phi' = 1/2$  with non-localised structures formed; (c)  $\zeta$  satisfies Eq. (5.11) and a localised structure is formed.*

It is worth noting that Eq. (5.11) only holds when

$$(5.12) \quad -1 \leq \cosh(2\pi S\phi') - 2\pi S\phi' \sinh(2\pi S\phi') \leq 1,$$

which numerically gives rise to a range for  $S\phi'$  by

$$(5.13) \quad 0 \leq S\phi' \leq 0.2465.$$

Actually, if we let  $X = \phi'\zeta$  and  $Y = \phi'S$ , Eq. (5.10) is of the same form as the equilibrium equations for a row of periodically distributed dipoles discussed by [19]. Following the same arguments by [19], we also draw the following conclusion concerning the stability of the obtained equilibrium structures.

1. Equilibrium Type I ( $\zeta = 0$ ), it is always unstable.
2. Equilibrium Type II ( $\phi'\zeta = 1/2$ ), it is only stable when Equilibrium Type III do not exist.
3. Equilibrium Type III ( $\zeta$  satisfies Eq. (5.11)), it is always stable.

Another way to investigate the stability of equilibrium states is by considering the energy per length denoted by  $E/L$  with respect to  $\zeta$ , the pair width scaled by  $N$ . In fact, an infinitesimal change in  $\zeta$  requires the work done by an amount of

$$(5.14) \quad d\left(\frac{E}{L}\right) = \frac{b\hat{\tau}_{\text{int}}^{(0)}}{2} \cdot \frac{d\zeta}{N}.$$

Hence

$$(5.15) \quad \frac{E}{L} = \frac{\log(\cosh(2\pi S\phi') - \cos(2\pi\zeta\phi'))}{4\pi\phi'N} + \frac{S \sinh(2\pi S\phi')}{2N(\cosh(2\pi S\phi') - \cos(2\pi\zeta\phi'))},$$

where the constant coming from integration is set to be 0.

A stable equilibrium state should correspond to a local minimum in  $E/L$  and the energy landscapes with respect to  $\zeta$  for different  $\phi'S$  are shown in Fig. 5.

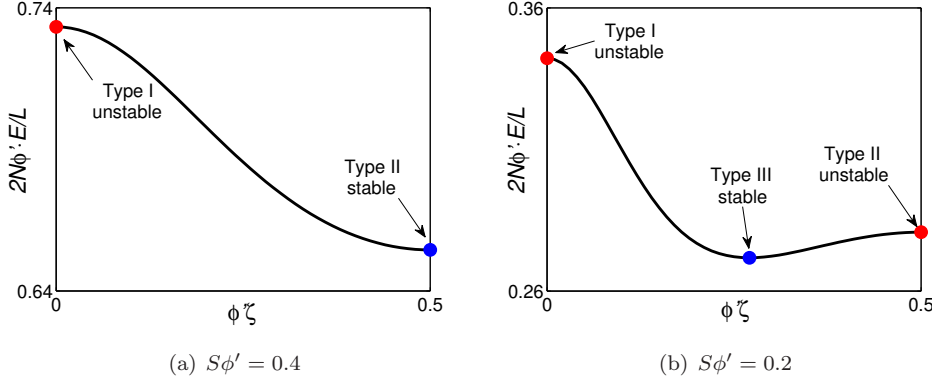


FIG. 5. (a) If  $S\phi'$  is larger than 0.2465, only two types of equilibria exist and Type II is the stable configuration. (b) If  $0 < S\phi' < 0.2465$ , a transition in stability from Type II to Type III takes place.

It is seen from the analysis above that a natural transition from a non-localised structure (Type II) to a localised structure (Type III) takes place as the slip plane spacing gets narrow. The discussion on the implementation to the formation of the persistent slip bands by such transition will be discussed in § 8.2 in a systematic manner.

**5.2.2. Equilibrium Type II: non-localised structures .** Now we derive for the equation for the pair density  $\phi'$  by simplifying Eq. (5.6) with the quantitative relation between  $\phi'$  and  $\zeta$  obtained. Here only stable configurations, i.e. Equilibrium Type II and III, are considered. When  $\phi'\zeta = 1/2$  (Type II), one can make use of the fact that  $(\phi'\zeta)' = 0$  and  $\sin(2\pi\phi'\zeta) = 0$ . This suggests that the terms associated with  $G_{12}$  and  $G_{13}$  in Eq. (5.9) both vanish. Therefore, the equation for  $\phi'$  can be obtained as

$$(5.16) \quad \begin{aligned} 0 &= \frac{2\phi''}{\phi'} \cdot G_{11}(\pi, 2\pi S\phi') + \frac{1}{2\phi'} \cdot \frac{\partial \hat{\tau}_{\text{ext}}^0}{\partial \hat{x}} + S \frac{\partial \hat{\tau}_{\text{ext}}^0}{\partial \hat{y}} \\ &= -\frac{\phi''}{\phi'} - 4\pi S\phi'' \tanh(\pi S\phi') + 5\pi^2 S^2 \phi' \phi'' \text{sech}^2(\pi S\phi') \\ &\quad - 2\pi^3 S^3 (\phi')^2 \phi'' \text{sech}^2(\pi S\phi') \tanh(\pi S\phi') + \frac{1}{2\phi'} \cdot \frac{\partial \hat{\tau}_{\text{ext}}^0}{\partial \hat{x}} + S \frac{\partial \hat{\tau}_{\text{ext}}^0}{\partial \hat{y}}. \end{aligned}$$

Eq. (5.16) quantitatively describes the pair density distribution, when all dipoles form non-local structures as shown in Fig. 4(b).

**5.2.3. Equilibrium Type III: localised structures.** For Equilibrium Type III, we can incorporate Eq. (5.11) into Eq. (4.23) to (4.25) to obtain

$$(5.17) \quad \begin{aligned} G_{11}^{III} &= G_{11}(\cos^{-1}(\cosh(2\pi S\phi') - 2\pi S\phi' \sinh(2\pi S\phi')), 2\pi S\phi') \\ &= \frac{\operatorname{csch}^2(2\pi S\phi')}{8} ((1 - (2\pi S\phi')^2)(1 - \cosh(4\pi S\phi')) + 4\pi S\phi' \sinh(4\pi S\phi')) \\ &\quad - \frac{\sqrt{2}\zeta \cosh(2\pi S\phi') \sqrt{4\pi S\phi' \sinh(4\pi S\phi') - (1 + (2\pi S\phi')^2) \sinh^2(4\pi S\phi')}}{4} \end{aligned}$$

$$(5.18) \quad \begin{aligned} G_{12}^{III} &= G_{12}(\cos^{-1}(\cosh(2\pi S\phi') - 2\pi S\phi' \sinh(2\pi S\phi')), 2\pi S\phi') \\ &= -\frac{\zeta \operatorname{csch}(2\pi S\phi') ((1 + (2\pi S\phi')^2) \sinh(2\pi S\phi') - 4\pi S\phi' \cosh(2\pi S\phi'))}{8\pi(S\phi')^2} \end{aligned}$$

and

$$(5.19) \quad \begin{aligned} G_{13}^{III} &= G_{13}(\cos^{-1}(\cosh(2\pi S\phi') - 2\pi S\phi' \sinh(2\pi S\phi')), 2\pi S\phi') \\ &= -\frac{\pi \coth(2\pi S\phi') \sqrt{2\pi S\phi' \sinh(4\pi S\phi') - (1 + (2\pi S\phi')^2) \sinh^2(2\pi S\phi')}}{2}. \end{aligned}$$

Hence one may re-write Eq. (5.9) with reference to Eq. (5.17) to (5.19) for the equation for  $\phi'$ :

$$(5.20) \quad \begin{aligned} 0 &= \frac{2\pi S^2 \phi' \phi'' \cosh(2\pi S\phi')}{\sqrt{2\pi S\phi' \sinh(4\pi S\phi') - (1 + (2\pi S\phi')^2) \sinh^2(2\pi S\phi')}} \cdot (G_{12}^{III} + G_{13}^{III}) \\ &\quad + \frac{2\phi''}{\phi'} \cdot G_{11}^{III} - \frac{\phi'' \zeta}{2\pi(\phi')^2} \cdot G_{13}^{III} + \frac{1}{2\phi'} \cdot \frac{\partial \hat{\tau}_{\text{ext}}^0}{\partial \hat{x}} + S \frac{\partial \hat{\tau}_{\text{ext}}^0}{\partial \hat{y}}. \end{aligned}$$

The above equation for  $\phi'$  for dipoles in Equilibrium Type III is too complicated to analyse. To find an equation for the pair density of simpler form, we consider the case when  $S \rightarrow 0$ . However, in this case, the expansion in Eq. (4.20) becomes singular. This indicates that the equation for  $\phi'$  for a small  $S$  should be derived under a different regime.

**5.2.4. Equilibria under extremely small slip plane gaps.** Now we focus on this extreme case of Equilibrium Type III, where  $\hat{s} \sim \mathcal{O}(1/N^2)$ . Thus one needs to rescale  $\hat{s}$  by

$$(5.21) \quad \hat{s} = \frac{S_0}{N^2}.$$

In this scenario, the expansion of  $\zeta$  should take the form of

$$(5.22) \quad \zeta \sim \frac{\zeta^{(1)}}{N} + \frac{\zeta^{(2)}}{N^2} + \dots.$$

The reason of employing the expansion given by Eq. (5.22) can also be seen by letting  $S \rightarrow 0$  in Eq. (5.11). It is then found that  $\zeta \sim S \rightarrow 0$ .

Incorporating Eq. (5.22) with (3.6) and (3.7), we can thus expand  $\hat{p}_n$  and  $\hat{q}_n$  near  $\hat{x}_n$  as

$$(5.23) \quad \hat{p}_n \sim \hat{x}_n - \frac{\zeta_n^{(1)}}{2N^2} - \frac{\zeta_n^{(2)}}{2N^3} + \dots, \quad \hat{q}_n \sim \hat{x}_n + \frac{\zeta_n^{(1)}}{2N^2} + \frac{\zeta_n^{(2)}}{2N^3} + \dots,$$

for any integer  $n \in [0, N]$ . The above expansion infers that as  $\hat{s} \sim \mathcal{O}(1/N^2)$ , the spacing between  $\hat{p}_n$  and  $\hat{q}_n$ , which is now  $\mathcal{O}(1/N^2)$ , is far smaller than the distance between  $\hat{p}_n$  or  $\hat{q}_n$  and any other pole. Hence it may be better to analyse the internal resolved shear stress field at  $(\hat{p}_n, 0)$  by decomposing it into a local and a global part, i.e.

$$(5.24) \quad \hat{\tau}_{\text{int}}(\hat{p}_n, 0) = \hat{\tau}_{\text{loc}}^{n+} + \hat{\tau}_{\text{others}}^{n+},$$

where the local contribution  $\hat{\tau}_{\text{loc}}^{n+}$  denotes the resolved shear stress due to its pair partner, the negative pole located at  $(\hat{q}_n, \hat{s})$  given by

$$(5.25) \quad \hat{\tau}_{\text{loc}}^{n+} = -\frac{(\hat{p}_n - \hat{q}_n)((\hat{p}_n - \hat{q}_n)^2 - (\frac{S_0}{N^2})^2)}{N((\hat{p}_n - \hat{q}_n)^2 + (\frac{S_0}{N^2})^2)}$$

and  $\hat{\tau}_{\text{others}}^{n+}$  denotes the resolved shear stress exerted at  $(p_n, 0)$  due to all other dislocations

$$(5.26) \quad \hat{\tau}_{\text{others}}^{n+} = \frac{1}{N} \sum_{\substack{j=0 \\ j \neq n}}^N \left( \frac{1}{\hat{p}_n - \hat{p}_j} - \frac{(\hat{p}_n - \hat{q}_j)((\hat{p}_n - \hat{q}_j)^2 - (\frac{S_0}{N^2})^2)}{((\hat{p}_n - \hat{q}_j)^2 + (\frac{S_0}{N^2})^2)^2} \right).$$

In a similar way,  $\hat{\tau}(\hat{q}_n, \hat{s})$  is also decomposed by

$$(5.27) \quad \hat{\tau}_{\text{int}}(\hat{q}_n, \hat{s}) = \hat{\tau}_{\text{loc}}^{n-} + \hat{\tau}_{\text{others}}^{n-},$$

where

$$(5.28) \quad \hat{\tau}_{\text{loc}}^{n-} = \hat{\tau}_{\text{loc}}^{n+} = -\frac{(\hat{p}_n - \hat{q}_n)((\hat{p}_n - \hat{q}_n)^2 - (\frac{S_0}{N^2})^2)}{N((\hat{p}_n - \hat{q}_n)^2 + (\frac{S_0}{N^2})^2)}$$

and

$$(5.29) \quad \hat{\tau}_{\text{others}}^{n-} = \frac{1}{N} \sum_{\substack{j=0 \\ j \neq n}}^N \left( \frac{(\hat{q}_n - \hat{p}_j)((\hat{q}_n - \hat{p}_j)^2 - (\frac{S_0}{N^2})^2)}{((\hat{q}_n - \hat{p}_j)^2 + (\frac{S_0}{N^2})^2)^2} - \frac{1}{\hat{q}_n - \hat{q}_j} \right).$$

Incorporating Eq. (5.23) with (5.25), we have the expansion that

$$(5.30) \quad \hat{\tau}_{\text{loc}}^{n+} \sim N \cdot \frac{\zeta_n^{(1)}(\zeta_n^{(1)})^2 - S_0^2}{((\zeta_n^{(1)})^2 + S_0^2)^2} - \frac{\zeta_n^{(2)}((\zeta_n^{(1)})^4 + 6S_0^2(\zeta_n^{(1)})^2 + S_0^4)}{((\zeta_n^{(1)})^2 + S_0^2)^3} + \mathcal{O}\left(\frac{1}{N}\right).$$

For  $\hat{\tau}_{\text{others}}^{n+}$ , one can replace  $n$  in Eq. (5.23) by  $j$  to get the expansion of  $\hat{p}_j$  and  $\hat{q}_j$  near  $\hat{x}_j$ . Then incorporating the expansion results into Eq. (5.26) and using the fact that  $|\hat{x}_j - \hat{x}_n| \sim \mathcal{O}(1/N) \gg 1/N^2$  for any  $j \neq n$ , we obtain the expansion for  $\hat{\tau}_{\text{others}}^{n+}$  as

$$(5.31) \quad \begin{aligned} \hat{\tau}_{\text{others}}^{n+} \sim & -\frac{1}{N^3} \cdot \sum_{\substack{j=0 \\ j \neq n}}^N \frac{(\zeta_j^{(1)})^2}{(\hat{x}_j - \hat{x}_n)^2} - \frac{1}{N^4} \cdot \sum_{\substack{j=0 \\ j \neq n}}^N \frac{(\zeta_j^{(2)})^2}{(\hat{x}_j - \hat{x}_n)^2} \\ & - \frac{1}{N^4} \cdot \left( \frac{\zeta_j^{(3)}}{(\hat{x}_j - \hat{x}_n)^2} + \frac{3S_0^2 - \zeta_n^{(1)}\zeta_j^{(1)}}{(\hat{x}_j - \hat{x}_n)^3} \right) + \dots \end{aligned}$$

Similarly,

$$(5.32) \quad \hat{\tau}_{\text{others}}^{n-} \sim -\frac{1}{N^3} \cdot \sum_{\substack{j=0 \\ j \neq n}}^N \frac{(\zeta_j^{(1)})^2}{(\hat{x}_j - \hat{x}_n)^2} - \frac{1}{N^4} \cdot \sum_{\substack{j=0 \\ j \neq n}}^N \frac{(\zeta_j^{(2)})^2}{(\hat{x}_j - \hat{x}_n)^2} \\ - \frac{1}{N^4} \cdot \left( \frac{\zeta_j^{(3)}}{(\hat{x}_j - \hat{x}_n)^2} - \frac{3S_0^2 - \zeta_n^{(1)}\zeta_j^{(1)}}{(\hat{x}_j - \hat{x}_n)^3} \right) + \dots.$$

Since  $|\hat{x}_j - \hat{x}_n|$  is no smaller than  $\mathcal{O}(1/N)$ ,  $\hat{\tau}_{\text{others}}^{n+}$  and  $\hat{\tau}_{\text{others}}^{n-}$  may both grow as big as  $\mathcal{O}(1/N)$ . This means that  $\hat{\tau}_{\text{loc}}^{n+}$  dominates at the leading and the next orders over  $\hat{\tau}_{\text{others}}^{n+}$  in Eq. (5.24) and so does  $\hat{\tau}_{\text{loc}}^{n-}$  over  $\hat{\tau}_{\text{others}}^{n-}$  in Eq. (5.27). Hence when the system is at its equilibrium, the  $\mathcal{O}(N)$  and  $\mathcal{O}(1)$  terms of  $\hat{\tau}_{\text{loc}}^{n+}$  in Eq. (5.25) should both vanish. Thus  $\zeta^{(1)}$  and  $\zeta^{(2)}$  are calculated to be

$$(5.33) \quad \zeta_n^{(1)} = S_0$$

and

$$(5.34) \quad \zeta_n^{(2)} = 0,$$

respectively.

Eq. (5.33) is the leading-order solution to  $\zeta$ , one of the two unknowns. For the other unknown  $\phi'$ , as suggested by the previous examples, it should come from the balance of the “stress gradient”, or in another word, the difference of the total resolved shear stress at  $(\hat{q}_n, \hat{s})$  and  $(\hat{p}_n, 0)$ . Mathematically, the equation for  $\phi'$  should come from

$$(5.35) \quad \hat{\tau}_{\text{others}}^{n-} - \hat{\tau}_{\text{others}}^{n+} + \hat{\tau}_{\text{ext}}(\hat{q}_n, \hat{s}) - \hat{\tau}_{\text{ext}}(\hat{p}_n, 0) = 0.$$

It is worth noting that the local contribution from  $\hat{\tau}_{\text{loc}}^{n+}$  cancels with  $\hat{\tau}_{\text{loc}}^{n-}$  according to Eq. (5.28).

By using Eq. (5.33) and (5.34), we subtract Eq. (5.32) by Eq. (5.31) to obtain the “internal stress gradient” by

$$(5.36) \quad \hat{\tau}_{\text{others}}^{n-} - \hat{\tau}_{\text{others}}^{n+} \sim \frac{1}{N^5} \cdot \sum_{\substack{j=0 \\ j \neq n}}^N \frac{4S_0^2}{(\hat{x}_j - \hat{x}_n)^3} + \mathcal{O}\left(\frac{1}{N^5}\right).$$

To evaluate the summation in Eq. (5.36), we again introduce an inner region given by

$$(5.37) \quad \left\{ \hat{x} \mid |\phi(\hat{t}, \hat{x}) - \phi(\hat{t}, \hat{x}_n)| \leq \frac{K}{N} \right\},$$

where  $K \sim \sqrt{N}$ . Similar as in § 4, the summation in Eq. (5.36) can be calculated as the super-position of an inner and an outer approximation.

For the inner approximation, we employ Eq. (4.11) and the respective sum in

Eq. (5.36) thus becomes

$$\begin{aligned}
(5.38) \quad & \frac{1}{N^5} \cdot \sum_{\substack{j=n-K \\ j \neq n}}^{n+K} \frac{4S_0^2}{(\hat{x}_j - \hat{x}_n)^3} \\
& \sim \frac{1}{N^2} \cdot \sum_{\substack{j=n-K \\ j \neq n}}^{n+K} \frac{4S_0^2}{(j-n)^3} + \frac{1}{N^3} \cdot \sum_{\substack{j=n-K \\ j \neq n}}^{n+K} \frac{6S_0^2 \phi'_n \phi''_n}{(j-n)^2} + \frac{1}{N^3} \cdot \sum_{\substack{j=n-K \\ j \neq n}}^{n+K} \frac{6S_0^2 (\phi''_n)^2}{j-n} + \mathcal{O}\left(\frac{K}{N^5}\right) \\
& \sim \frac{2\pi^2 S_0^2 \phi'_n \phi''_n}{N^3} + \mathcal{O}\left(\frac{1}{N^3 K}\right).
\end{aligned}$$

where the estimation

$$(5.39) \quad \sum_{\substack{j=-K \\ j \neq 0}}^K \frac{1}{j^2} \sim \frac{\pi^2}{3} + \frac{2}{K} + \mathcal{O}\left(\frac{1}{K^2}\right)$$

is used. Eq. (5.38) suggests that the leading order estimation to  $\hat{\tau}_{\text{others}}^{n-} - \hat{\tau}_{\text{others}}^{n+}$  from the inner region is  $\mathcal{O}(1/N^3)$ .

Outside the inner region, we again use the Euler-Maclaurin formula to obtain

$$\begin{aligned}
(5.40) \quad & \frac{1}{N^5} \cdot \left( \sum_{j=0}^{n-K-1} \frac{4S_0^2}{(\hat{x}_n - \hat{x}_j)^3} + \sum_{j=n+K+1}^N \frac{4S_0^2}{(\hat{x}_n - \hat{x}_j)^3} \right) \\
& \sim \frac{4S_0^2}{N^4} \cdot \left( \int_{\hat{x}_0}^{\hat{x}_{n-K-1}} \frac{da}{(\hat{x}_n - a)^3} + \int_{\hat{x}_{n+K+1}}^{\hat{x}_n} \frac{da}{(\hat{x}_n - a)^3} \right) + \mathcal{O}\left(\frac{1}{N^2 K^3}\right) \\
& \sim \frac{4S_0^2}{N^4} \cdot \left( \frac{\phi'(\hat{x}_{n+K+1})}{2(\hat{x}_n - \hat{x}_{n+K+1})^2} - \frac{\phi'(\hat{x}_{n-K-1})}{2(\hat{x}_n - \hat{x}_{n-K-1})^2} - \frac{\phi''(\hat{x}_{n+K+1})}{\hat{x}_n - \hat{x}_{n+K+1}} + \frac{\phi''(\hat{x}_{n-K-1})}{\hat{x}_n - \hat{x}_{n-K-1}} \right) \\
& + \frac{4S_0^2}{N^4} \cdot \left( \int_{\hat{x}_0}^{\hat{x}_{n-K-1}} \frac{\phi'''(a) da}{\hat{x}_n - a} + \int_{\hat{x}_{n+K+1}}^{\hat{x}_n} \frac{\phi'''(a) da}{\hat{x}_n - a} \right) + \mathcal{O}\left(\frac{1}{N^2 K^3}\right)
\end{aligned}$$

In analogy to the previous case, since  $|\hat{x}_{n-K-1} - \hat{x}_n|$  and  $|\hat{x}_{n+K+1} - \hat{x}_n|$  are both of  $\mathcal{O}(K/N)$ , one can use the expansion in Eq. (4.44) and (4.45) to further simplify the outcome of Eq. (5.40) to obtain

$$(5.41) \quad \frac{1}{N^5} \cdot \left( \sum_{j=0}^{n-K-1} \frac{4S_0^2}{(\hat{x}_n - \hat{x}_j)^3} + \sum_{j=n+K+1}^N \frac{4S_0^2}{(\hat{x}_n - \hat{x}_j)^3} \right) \sim \mathcal{O}\left(\frac{1}{N^2 K^3}, \frac{1}{N^3 K}\right).$$

Eq. (5.41) implies that the contribution to  $\hat{\tau}_{\text{others}}^{n-} - \hat{\tau}_{\text{others}}^{n+}$  from all pole pairs, whose centers fall outside the inner region is only  $o(1/N^3)$ . This is negligible compared to the estimation made from the inner region.

Therefore, incorporating Eq. (5.38) with (5.36), we obtain the asymptotic expression for the internal stress gradient at  $\hat{x}_n$  by

$$\begin{aligned}
(5.42) \quad \hat{\tau}_{\text{others}}^{n-} - \hat{\tau}_{\text{others}}^{n+} & \sim \frac{2\pi^2 S_0^2 \phi'_n \phi''_n}{N^3} + o\left(\frac{1}{N^3}\right) \\
& \sim \frac{2\pi^2 S^2 \phi'_n \phi''_n}{N} + o\left(\frac{1}{N^3}\right),
\end{aligned}$$

where for the purpose of being uniform  $S_0 = NS$  is used with reference to Eq. (3.5) and (5.21).

With  $\zeta^{(1)} = S_0$  calculated from Eq. (5.33), the externally applied “stress gradient” can be asymptotically evaluated by

$$(5.43) \quad \begin{aligned} \hat{\tau}_{\text{ext}}(\hat{q}_n, \hat{s}) - \hat{\tau}_{\text{ext}}(\hat{p}_n, 0) &\sim \frac{S_0}{N^2} \cdot \left( \frac{\partial \hat{\tau}_{\text{ext}}}{\partial \hat{x}} \Big|_{(\hat{x}_n, 0)} + \frac{\partial \hat{\tau}_{\text{ext}}}{\partial \hat{y}} \Big|_{(\hat{x}_n, 0)} \right) + o\left(\frac{1}{N^2}\right) \\ &\sim \frac{S}{N} \cdot \left( \frac{\partial \hat{\tau}_{\text{ext}}^0(\hat{x}_n)}{\partial \hat{x}} + \frac{\partial \hat{\tau}_{\text{ext}}^0(\hat{x}_n)}{\partial \hat{y}} \right) + o\left(\frac{1}{N^2}\right), \end{aligned}$$

where Eq. (4.59), (4.61) and  $S_0 = NS$  are used.

Incorporating Eq. (5.42) and (5.43) with Eq. (5.35), the equation for the pair density  $\phi'$  is obtained

$$(5.44) \quad 2\pi^2 S^2 \phi' \phi'' + S \cdot \left( \frac{\partial \hat{\tau}_{\text{ext}}^0}{\partial \hat{x}} + \frac{\partial \hat{\tau}_{\text{ext}}^0}{\partial \hat{y}} \right) = 0,$$

for the case when  $S$  is small. Here  $\zeta$ , according to its leading-order solution given by Eq. (5.33)

$$(5.45) \quad \zeta = S.$$

If we define in this scenario that

$$(5.46) \quad \hat{\tau}_{\text{opp}}^{(1)}(\hat{x}) = \pi^2 S^2 \phi' \phi'',$$

Eq. (5.44) is of the same form as Eq. (5.4).

Compared to the equation for  $\phi'$  in § 5.2.3, Eq. (5.44) is much simpler. Actually, it will be shown from the numerical examples later that one can use Eq. (5.33) and (5.44) to approximately describe the collective behaviour of the dipole system where localised structures are formed. It is worth noting that if  $\partial \hat{\tau}_{\text{ext}}^0 / \partial \hat{x} = 0$ , Eq. (5.44) agrees with the result by [9], where each dipole pair is treated as one object and discrete-to-continuum transition is performed.

**5.2.5. Summary.** To summarise, a row of dipoles may form two types of stable equilibrium states depending on the spacing between the two slip planes under almost zero-applied-stress.

When  $\phi' S \geq 0.2465$ , the equations for the two field variables of interest are

$$(5.47) \quad \zeta = \frac{1}{2\phi'}$$

and

$$(5.48) \quad \begin{aligned} 0 = &-\frac{\phi''}{\phi'} - 4\pi S \phi'' \tanh(\pi S \phi') + 5\pi^2 S^2 \phi' \phi'' \text{sech}^2(\pi S \phi') \\ &- 2\pi^3 S^3 (\phi')^2 \phi'' \text{sech}^2(\pi S \phi') \tanh(\pi S \phi') + \frac{1}{2\phi'} \cdot \frac{\partial \hat{\tau}_{\text{ext}}^0}{\partial \hat{x}} + S \frac{\partial \hat{\tau}_{\text{ext}}^0}{\partial \hat{y}}. \end{aligned}$$

When  $0 < \phi' S < 0.2465$ , the governing equations at the coarse-grained level are

$$(5.49) \quad \zeta = S$$

and

$$(5.50) \quad 2\pi^2 S \phi' \phi'' + \frac{\partial \hat{\tau}_{\text{ext}}^0}{\partial x} + \frac{\partial \hat{\tau}_{\text{ext}}^0}{\partial y} = 0.$$

This agrees with the results by [9].

**5.3. Equilibria under arbitrarily externally applied stresses.** Now we consider the case when the leading order of the externally applied resolved shear stress is non-zero, i.e.  $\tau_{\text{ext}}^0 \sim \mathcal{O}(1)$ , provided  $S \sim \mathcal{O}(1)$ . In this case, Eq. (5.5) becomes

$$(5.51) \quad \begin{aligned} 0 &= G_0(2\pi\phi'\zeta, 2\pi\phi'S) + \frac{\tau_{\text{ext}}^0}{\pi\phi'} \\ &= \frac{\sin(2\pi\phi'\zeta)}{\cosh(2\pi S\phi') - \cos(2\pi\phi'\zeta)} \cdot \left(1 - \frac{2\pi S\phi' \sinh(2\pi S\phi')}{\cosh(2\pi S\phi') - \cos(2\pi\phi'\zeta)}\right) + \frac{\hat{\tau}_{\text{ext}}^0}{\pi\phi'}. \end{aligned}$$

Compared to the almost-zero-external-stress case, it is not easy to explicitly express  $\zeta$  in terms of  $\phi'$  by solving Eq. (5.51). However, some analysis can still be done to understand the resulting equilibrium patterns.

Eq. (5.51) can be considered as a function implicitly determined by  $\zeta\phi'$ ,  $S\phi'$  and  $\hat{\tau}_{\text{ext}}^0/\phi'$ . Actually from the first line of Eq. (5.51), if we examine the behaviour of  $G_0$  in  $(\zeta\phi') - (S\phi')$  plane, all pairs of  $(\phi'\zeta, \phi'S)$  on the contours of  $-G_0(2\pi\phi'\zeta, 2\pi\phi'S)$  with height  $\hat{\tau}_{\text{ext}}^0/(\pi\phi')$  should satisfy Eq. (5.51) as shown in Fig. 6. It is worth noting

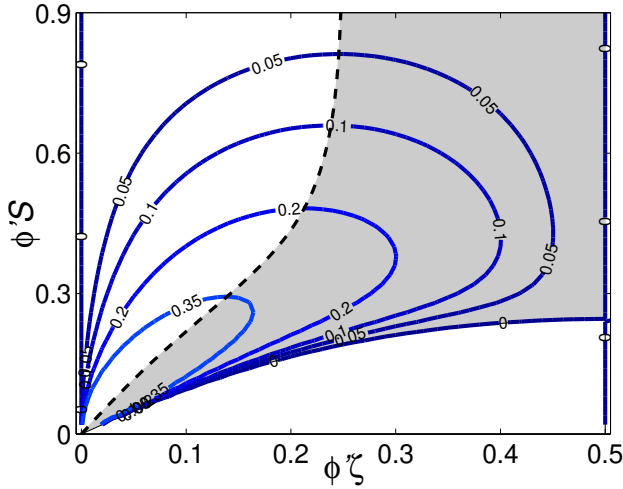


FIG. 6. The contours of  $-G_0(2\pi\phi'\zeta, 2\pi\phi'S)$  taken at various heights given by  $\hat{\tau}_{\text{ext}}^0/(\pi\phi')$ . The shaded region corresponds to stable configurations and the dashed curve is drawn from Eq. (5.53)

that here only  $\hat{\tau}_{\text{ext}}^0 > 0$  is considered. This is because if  $\hat{\tau}_{\text{ext}}^0 < 0$ , we simply let  $\zeta < 0$  and same conclusion will be drawn.

Two points are worth being addressed from Fig. 6. Firstly, given  $\hat{\tau}_{\text{ext}}^0/\phi'$  there exists a maximised  $\phi'S^*$  and its corresponding value for  $\zeta$  is denoted by  $\zeta^*$ . To find the pair of  $\zeta^*$  and  $S^*$ , we take the derivatives on both sides of Eq. (5.51) with respect to  $\zeta\phi'$  and obtain

$$(5.52) \quad \frac{\partial G_0(2\pi\phi'\zeta, 2\pi\phi'S)}{\partial(\zeta\phi')} + \frac{\partial G_0(2\pi\phi'\zeta, 2\pi\phi'S)}{\partial(\phi'S)} \cdot \frac{\partial(\phi'S)}{\partial(\phi'\zeta)} = 0.$$

Here  $\partial(\phi'S)/\partial(\phi'\zeta)$  should vanish at  $(\phi'\zeta^*, \phi'S^*)$  according to the definition of  $S^*$ .

Thus Eq. (5.52) can be re-written by

$$(5.53) \quad 0 = \frac{\cos(2\pi\zeta^*\phi')}{\cosh(2\pi S^*\phi') - \cos(2\pi\zeta^*\phi')} \cdot \left(1 - \frac{2\pi S^*\phi' \sinh(2\pi S^*\phi')}{\cosh(2\pi S^*\phi') - \cos(2\pi\zeta^*\phi')}\right) - \frac{\sin^2(2\pi\zeta^*\phi')}{(\cosh(2\pi S^*\phi') - \cos(2\pi\zeta^*\phi'))^2} + \frac{4\pi S^*\phi' \sin^2(2\pi\zeta^*\phi') \sinh(2\pi S^*\phi')}{(\cosh(2\pi S^*\phi') - \cos(2\pi\zeta^*\phi'))^3}.$$

Eq. (5.53) implicitly gives the relation between  $\zeta^*$  and  $S^*$ , which produces the dashed curve in Fig. 6.

The second observation from Fig. 6 is that given  $\hat{\tau}_{\text{ext}}^0$ , there are two choices for  $\phi'\zeta$  for any  $S < S^*$ . It is suggested by [19] that only  $\zeta$  larger than  $\zeta^*$  gives rise to a stable equilibrium state. This implies that only  $(\phi'\zeta, \phi'S)$  falling into the shaded region in Fig. 6 correspond to stable configurations.

The above analysis provides us some insight to the equilibrium configurations. Nevertheless, to find  $\zeta$  and  $\phi'$  satisfying Eq. (5.1) and (5.4), one has to turn to numerical approaches. In fact, it will be seen in the next section that the equilibrium solutions for  $\zeta$  and  $\phi'$  are effectively the steady state solutions to the derived dynamical equations derived in the next section.

When  $S \rightarrow 0$ , we still use Eq. (5.49) and (5.50) as the governing equations for  $\zeta$  and  $\phi'$ , respectively. This is because when a positive pole is very close to its pair partner, their mutual interaction is so strong that a mild externally applied stress ( $\hat{\tau}_{\text{ext}}^{(0)} \sim \mathcal{O}(1)$ ) can be negligible.

**6. Dynamics at the continuum level.** Now we consider the formulation of the discrete dislocation pole dynamics governed by Eq. (3.1) to (3.4) at the coarse-grained level.

If we plug Eq. (4.62) into the law of motion in Eq. (3.1), the  $n$ -th positive pole can be asymptotically we can asymptotically captured by

$$(6.1) \quad \frac{d\hat{p}_n}{dt} \sim \hat{\tau}_{\text{int}}^{(0)}(\hat{x}_n) + \hat{\tau}_{\text{ext}}^0(\hat{x}_n) + \frac{1}{N} \left( \hat{\tau}_{\text{same}}^{(1)}(\hat{x}_n) - \hat{\tau}_{\text{opp}}^{(1)}(\hat{x}_n) + \frac{\zeta}{2} \frac{\partial \hat{\tau}_{\text{ext}}^0(\hat{x}_n)}{\partial \hat{x}} \right) + o\left(\frac{1}{N}\right)$$

Analogously, the motion of the  $n$ -th negative pole is governed by

$$(6.2) \quad \frac{d\hat{q}_n}{dt} \sim -\hat{\tau}_{\text{int}}^{(0)}(\hat{x}_n) - \hat{\tau}_{\text{ext}}^0(\hat{x}_n) - \frac{\hat{\tau}_{\text{same}}^{(1)}(\hat{x}_n) + \hat{\tau}_{\text{opp}}^{(1)}(\hat{x}_n)}{N} - \frac{\zeta}{2N} \cdot \frac{\partial \hat{\tau}_{\text{ext}}^0(\hat{x}_n)}{\partial \hat{x}} - \frac{S}{N} \cdot \frac{\partial \hat{\tau}_{\text{ext}}^0(\hat{x}_n)}{\partial \hat{y}} + o\left(\frac{1}{N}\right).$$

Now we look for the evolutionary equation for the two field variables  $\phi$  and  $\zeta$ . We know that  $\phi(\hat{t}, \hat{x}_n) = n/N$  by definition. Thus taking full derivatives on its both sides with respect to  $\hat{t}$  gives rise to

$$(6.3) \quad \frac{\partial \phi_n}{\partial \hat{t}} + \frac{d\hat{x}_n}{d\hat{t}} \cdot \frac{\partial \phi_n}{\partial \hat{x}} = 0.$$

According to the definition of  $\hat{x}_n$  given by Eq. (3.6), we have

$$(6.4) \quad \frac{d\hat{x}_n}{d\hat{t}} = \frac{d\hat{p}_n}{d\hat{t}} + \frac{d\hat{q}_n}{d\hat{t}} \sim -\frac{1}{N} \left( 2\hat{\tau}_{\text{opp}}^{(1)}(\hat{x}_n) + \zeta \cdot \frac{\partial \hat{\tau}_{\text{ext}}^0(\hat{x}_n)}{\partial \hat{x}} + S \cdot \frac{\partial \hat{\tau}_{\text{ext}}^0(\hat{x}_n)}{\partial \hat{y}} \right) + o\left(\frac{1}{N}\right),$$

where Eq. (6.1) and (6.2) are employed. Incorporating Eq. (6.4) with (6.3) gives

$$(6.5) \quad \frac{\partial \phi}{\partial \hat{t}} - \frac{1}{N} \left( 2\hat{\tau}_{\text{opp}}^{(1)} + \zeta \cdot \frac{\partial \hat{\tau}_{\text{ext}}^0}{\partial \hat{x}} + S \cdot \frac{\partial \hat{\tau}_{\text{ext}}^0}{\partial \hat{y}} \right) \cdot \frac{\partial \phi}{\partial \hat{x}} \sim o(1),$$

where the subscript  $n$  is dropped and Eq. (6.5) can be considered as the evolutionary equation for  $\phi$  in an asymptotical sense.

Similarly, according to Eq. (3.7), we have

$$(6.6) \quad \frac{\partial \zeta_n}{\partial \hat{t}} + \frac{d\hat{x}_n}{d\hat{t}} \cdot \frac{\partial \zeta_n}{\partial \hat{x}} = \frac{d\zeta_n}{dt} = N \cdot \left( \frac{d\hat{q}_n}{d\hat{t}} - \frac{d\hat{p}_n}{d\hat{t}} \right).$$

Then combining Eq. (6.1), (6.2), (6.4) and (6.6) and dropping the subscript  $n$ , we asymptotically derive for an equation for  $\zeta$  as

$$(6.7) \quad \frac{\partial \zeta}{\partial \hat{t}} \sim -2N \cdot (\tau_{\text{int}}^{(0)} + \tau_{\text{ext}}^{(0)}) + \mathcal{O}(1).$$

It can be observed from Eq. (6.5) and Eq (6.7) that the time scales associated with both  $\phi$  and  $\zeta$  need to be reset to facilitate further asymptotic analysis. This is achieved by introducing a fast temporal variable  $\hat{t}_f$  given by

$$(6.8) \quad \hat{t}_f = \frac{\hat{t}}{N}$$

and a slow temporal variable  $\hat{t}_s$  given by

$$(6.9) \quad \hat{t}_s = N\hat{t}.$$

Hence the leading order effects of Eq. (6.5) and (6.7) can be formulated by

$$(6.10) \quad \frac{\partial \phi}{\partial \hat{t}_s} - \left( 2\hat{\tau}_{\text{opp}}^{(1)} + \zeta \cdot \frac{\partial \hat{\tau}_{\text{ext}}^0}{\partial \hat{x}} + S \cdot \frac{\partial \hat{\tau}_{\text{ext}}^0}{\partial \hat{y}} \right) \cdot \frac{\partial \phi}{\partial \hat{x}} = 0$$

and

$$(6.11) \quad \frac{\partial \zeta}{\partial \hat{t}_f} = -2\tau_{\text{int}}^{(0)} - 2\tau_{\text{ext}}^{(0)},$$

respectively.

The discrepancy in the evolving speed of  $\zeta$  and  $\phi$  can be interpreted as follows. When observed at the time scale characterised by  $\hat{t}_s$ , at which  $\phi$  evolves, the evolution of  $\zeta$  is too quick to be captured before the steady state is reached. This means the dynamical problems at the continuum level can be effectively tracked by the evolution of  $\phi$  (of time scale by  $\hat{t}_s$ ) with equilibrium state of  $\zeta$  implicitly determined by Eq. (5.51). Therefore, the discrete dislocation pole dynamics discussed in this paper can be re-formulated by an equilibrium equation given by

$$(6.12) \quad \hat{\tau}_{\text{int}}^{(0)} + \hat{\tau}_{\text{ext}}^{(0)} = 0$$

and an evolution equation given by Eq. (6.10) at the coarse-grained scale.

As indicated by the case of equilibrium problems discussed in § (5), there are two different regimes in the determination of the expressions of  $\hat{\tau}_{\text{int}}^{(0)}$  and  $\hat{\tau}_{\text{opp}}^{(1)}$  characterised by slip plane gaps.

When  $S$  is not small, i.e.  $S \sim \mathcal{O}(1)$ , Eq. (6.12) is effectively Eq. (5.51)

$$(6.13) \quad \frac{\sin(2\pi\phi'\zeta)}{\cosh(2\pi S\phi') - \cos(2\pi\phi'\zeta)} \cdot \left(1 - \frac{2\pi S\phi' \sinh(2\pi S\phi')}{\cosh(2\pi S\phi') - \cos(2\pi\phi'\zeta)}\right) + \frac{\hat{\tau}_{\text{ext}}^0}{\pi\phi'} = 0$$

and  $\hat{\tau}_{\text{opp}}^{(1)}$  in Eq. (6.10) satisfies

$$(6.14) \quad \hat{\tau}_{\text{opp}}^{(1)} = \frac{\phi''}{\phi'} G_{11}(2\pi\phi'\zeta, 2\pi\phi'S) + (\phi'\zeta)' G_{12}(2\pi\phi'\zeta, 2\pi\phi'S) + \phi'\zeta' G_{13}(2\pi\phi'\zeta, 2\pi\phi'S).$$

For a small  $S$ , we refer to the case studied in § 5.2.4. Again the assumption that a mild external stress can not alter the width of a pair of dipole too much is used. Hence we set approximately the equilibrium equation for  $\zeta$  to be Eq. (5.49)

$$(6.15) \quad \zeta = S.$$

The expression for  $\hat{\tau}_{\text{opp}}^{(1)}$  is then determined by

$$(6.16) \quad \hat{\tau}_{\text{opp}}^{(1)} = \pi^2 S^2 \phi'' \phi',$$

with reference to Eq. (5.46).

**7. Numerical results.** In this section, we compare the numerical results by applying the derived continuum model with what are obtained by using its underlying discrete dislocation dynamical model. For simplicity, we here consider the case when  $\partial\hat{\tau}_{\text{ext}}^0/\partial\hat{x} = 0$  and  $\partial\hat{\tau}_{\text{ext}}^0/\partial\hat{y}$  is a constant. All simulation results shown were carried out by using Matlab (R2010a).

**7.1. Equilibria.** We first compare the equilibrium state solutions between the discrete and continuum models for the almost-zero-externally-applied stress case. In this scenario, there are analytical solutions from the continuum model. As for the 2D DDD model, the evolution is governed by  $2(N+1)$  ordinary differential equations given by Eq. (3.1) to (3.4). We discretise the temporal derivatives using the Euler scheme, e.g.

$$(7.1) \quad \left. \frac{d\hat{p}_n}{d\hat{t}} \right|_{t_0} = \frac{\hat{p}_n(t_0 + \Delta t_{\text{dis}}) - \hat{p}_n(t_0)}{\Delta t_{\text{dis}}},$$

where  $\Delta t_{\text{dis}}$  is the time step. It has been posteriorly seen that we need

$$(7.2) \quad \Delta t_{\text{dis}} < \frac{C}{N},$$

where  $C$  is some number, to ensure the convergence of the implemented numerical scheme. All DDD simulation results shown here start with  $N+1$  pairs of dislocations, which are uniformly distributed within  $[0, 1]$ . At the two boundaries, we fix  $\hat{p}_0 = \hat{q}_0 = 0$  and  $\hat{p}_N = \hat{q}_N = 1$ . The simulation is stopped when the change within a new time step drops below  $10^{-5}\Delta t_{\text{dis}}$ . It is worth noting that in all figures presented in this section, results by the continuum model are represented by solid curves, while results by the DDD model are represented by dotted-curves.

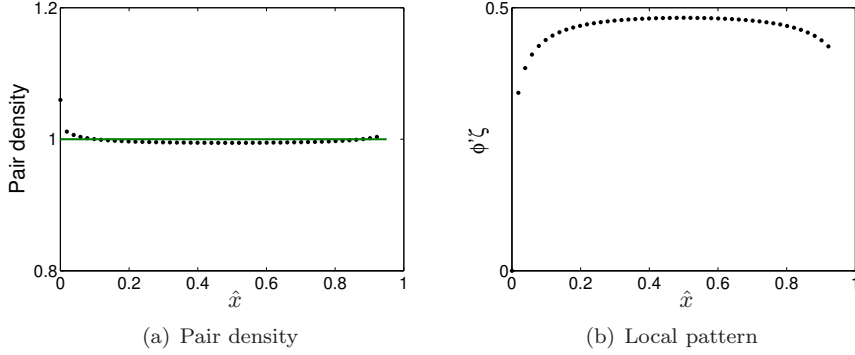


FIG. 7. Comparison of the pair density and the pair width with the results from the DDD models in the absence of applied stress gradient. When  $S = 0.3$ , the system forms Equilibrium Type II. Here  $N = 50$ ,  $\Delta t_{dis} = 2 \times 10^{-3}$ , and it takes roughly  $2 \times 10^4$  to attain an error of  $10^{-5} \Delta t_{dis}$ . The value of  $\phi' \zeta$  predicted by the continuum model is 0.5.

**7.1.1. Equilibrium Type II: non-localised structures.** To see Equilibrium Type II, according to Eq. (5.13), one needs a relative large  $S$ , which is chosen to be 0.3 here.

When there is no externally applied stress gradient, the derived continuum model predicts  $\phi' = 1$  and  $\phi' \zeta = 1/2$ . A comparison of these values with that from DDD simulation is shown in Fig. 7. The pair density at  $\hat{x}_n$  by the DDD model is calculated by  $1/(N(\hat{x}_{n+1} - \hat{x}_n))$ . It can be seen from Fig. 7 that the values from the two models agree well away from the boundaries. The deviation near the two ends are induced by the boundary image effect. In Fig. 8, the dipolar arrangement at equilibrium from the DDD simulation is shown and uniform distribution can be seen.

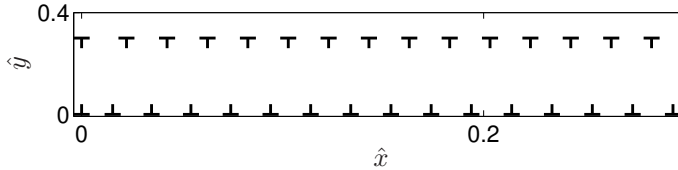


FIG. 8. When  $S = 0.3$ , all dipoles are uniformly distributed with Equilibrium Type II formed.

When the a non-vanishing stress-gradient, say,  $\partial \hat{\tau}^0 / \partial \hat{y} = 1$  here, is applied system, we can integrate Eq. (5.48) with respect to  $\hat{x}$  to implicitly express the pair density  $\phi'$  by

$$(7.3) \quad \log \left( \frac{\cosh(\pi \phi' S)}{\phi'} \right) + \left( \frac{\pi \phi' S}{\cosh(\pi \phi' S)} \right)^2 + 3\pi \phi' S \tanh(\pi \phi' S) = C - \frac{\partial \hat{\tau}^0}{\partial \hat{y}} \cdot S \hat{x},$$

where  $C$  is a constant to be determined by  $\int_0^1 \phi' d\hat{x} = 1$ . The pair density distribution based on Eq. (7.3) is drawn in Fig. 9(a) and good agreement with the numerical results in both pair density and  $\phi' \zeta$  are seen in the middle of the computational domain.

**7.1.2. Localised equilibria.** We also compare the simulation results for equilibrium states of Type III by choosing  $S = 0.1$  and  $N = 50$ . The comparison results under a vanishing applied stress-gradient is shown in Fig. 10. In this case,  $\zeta$  is calcu-

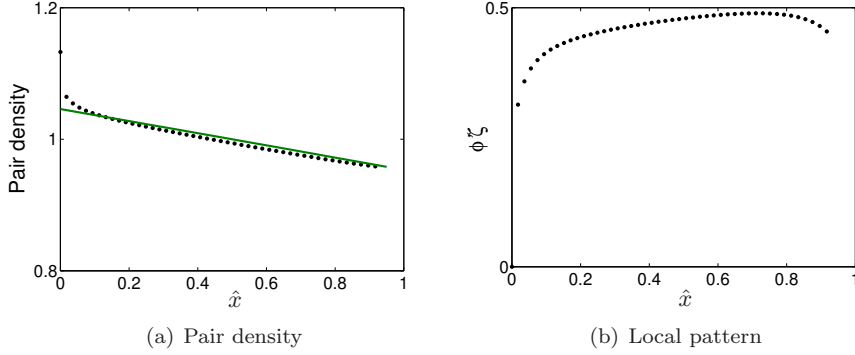


FIG. 9. *Dipoles of Equilibrium Type II pile-up against applied stress gradient. Here  $S = 0.3$ ,  $\partial\hat{\tau}^0/\partial\hat{y} = 1$ ,  $N = 50$ ,  $\Delta t_{dis} = 2 \times 10^{-3}$ . It takes roughly  $2 \times 10^4$  to attain an error of  $10^{-5} \Delta t_{dis}$ .*

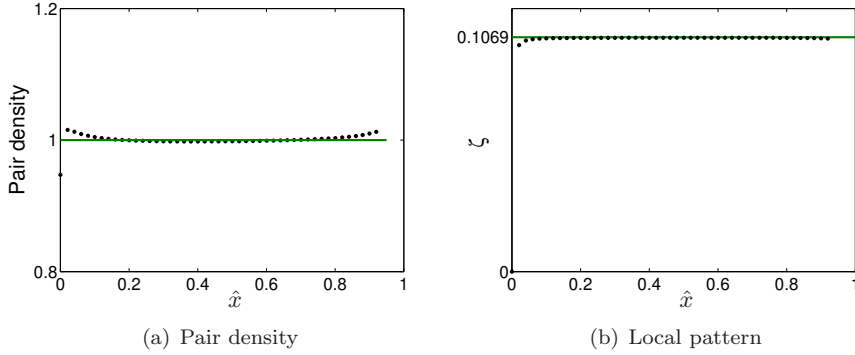


FIG. 10. *Comparison of the pair density and the pair width with the results from the DDD models in the absence of applied stress gradients. When  $S = 0.1$ , the system takes the equilibrium state of Type III. Here  $N = 50$ ,  $\partial\hat{\tau}^0/\partial\hat{y} = 1$ ,  $\Delta t_{dis} = 2 \times 10^{-4}$  and it takes roughly  $6.7 \times 10^5$  to attain an error of  $10^{-5}$ .*

lated to be 0.1069 with reference to Eq. (5.11), and this is very close to our predicted value, which is  $\zeta = S = 0.1$ . The dipolar arrangement is shown in Fig. 11.

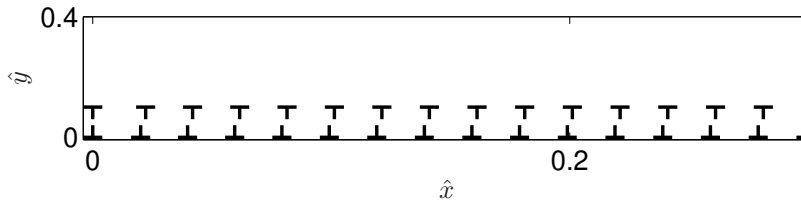


FIG. 11. *Uniform-density dislocation structures in the absence of applied stress-gradient from the DDD simulation of Equilibrium Type III.*

When the applied stress-gradient is given by  $\partial\hat{\tau}^0/\partial\hat{x} = 1$ , the pair density distri-

bution  $\phi'$  can be solved from Eq. (5.50)

$$(7.4) \quad \phi' = \frac{1}{\pi S} \sqrt{C - \frac{\partial \hat{\tau}^0}{\partial \hat{y}} \cdot S \hat{x}},$$

where  $C$  is also determined by  $\int_0^1 \phi' d\hat{x} = 1$ . In Fig. 12, the comparison of the pair density distribution and the pair width between the two models are shown and mutual agreement is observed.

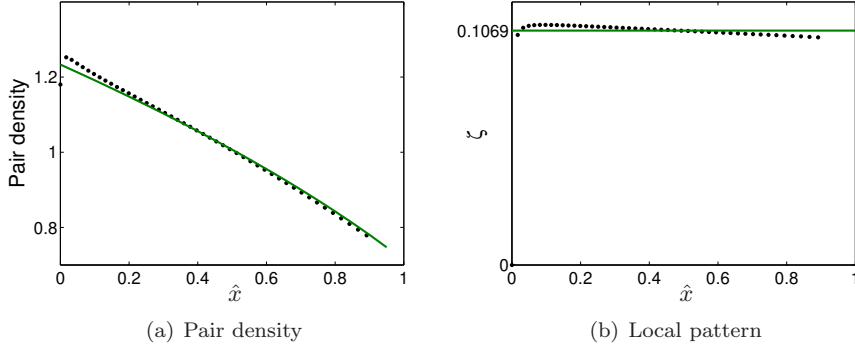


FIG. 12. Dipole of Equilibrium Type III pile-up against an applied stress gradient. Here  $S = 0.1$ ,  $\partial \hat{\tau}^0 / \partial \hat{y} = 1$ ,  $N = 50$ ,  $\Delta t_{dis} = 2 \times 10^{-4}$ . It takes roughly  $1.4 \times 10^6$  to attain an error of  $10^{-5} \Delta t_{dis}$ .

**7.1.3. Equilibria of Mixed Types.** When  $S = 0.24$ , it can be seen from Fig. 13 that Equilibrium Type II and III co-exist at the steady state. Near the left boundary,

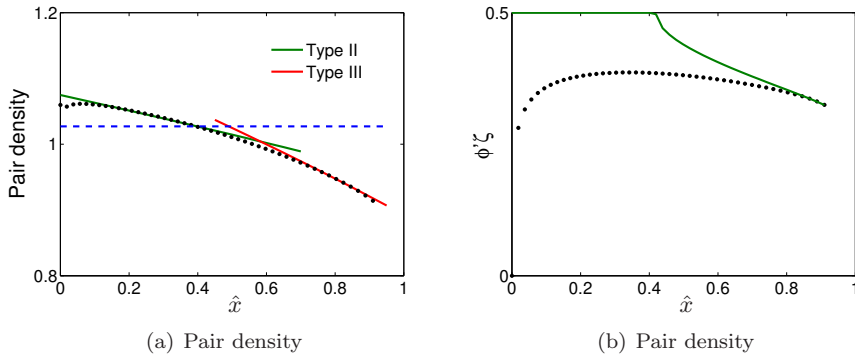


FIG. 13. Dipole of mixed equilibrium types pile-up against stress gradient. Near the left boundary, the dipoles take the equilibrium of Type II. A natural transition from Type II to III is seen roughly where the pair density drops below  $0.2456/0.24 \approx 1.03$ , which is characterised by the horizontal dash line. Here  $S = 0.24$ ,  $\hat{\tau}^0 = \hat{y}$ ,  $N = 50$ ,  $\Delta t_{dis} = 5 \times 10^{-4}$ . It takes roughly  $9 \times 10^4$  to attain an error of  $10^{-5} \Delta t_{dis}$ .

all dipoles are of Equilibrium of Type II. A transition from Type II to III should take place when the condition (5.13) holds. In this scenario, the transition should happen when the pair density drops below some critical value (the dashed line in Fig. 13)

given by

$$\phi' = \frac{0.2465}{S} \approx 1.03.$$

It can be seen from Fig. 13 that values of the pair density agree well with each for both cases, while there is roughly a 20% variance in  $\phi'\zeta$  for Equilibrium Type II.

**7.2. Dynamics.** Then we compare simulation results by applying the derived continuum model and the DDD model to same dynamical processes. All simulations start with  $N + 1$  pairs of dislocations and two ends locked in  $[0, 1]$ . For simulations at the level of the discrete dislocations, the set-ups and procedures are taken in a same manner as in § 7.1. For simulations using the derived continuum model, the computational domain  $[0, 1]$  is discretised with grid size  $\Delta x$ , while the temporal derivative is also discretised using the Euler method with time step  $\Delta t_{\text{con}}$ . At each time step, we take the following procedure

$$(7.5) \quad \phi \xrightarrow{\text{central difference}} \phi' \xrightarrow{\text{Eq. (6.13) or (6.15)}} \zeta \xrightarrow{\text{Eq. (6.10)}} \phi.$$

It is worth noting that the Courant-Friedrichs-Lewy (CFL) condition is needed when discretising Eq. (6.10). This is because Eq. (6.10) is actually of (non-linear) parabolic type given the existence of  $\phi''$  in  $\hat{\tau}_{\text{opp}}^{(1)}$ . The CFL condition adopted for the simulation results presented in this paper is

$$(7.6) \quad \Delta t_{\text{con}} = C\Delta x^2,$$

where  $C$  is chosen to be 1.25.

The parameters chosen for the first set of numerical examples are  $S = 0.3$ ,  $\hat{\tau}_{\text{ext}}^0 = 0.5$  and  $\partial\hat{\tau}_{\text{ext}}^0/\partial\hat{y} = 1$ . Since  $S$  is not small here, the governing equations are given by Eq. (6.10), (6.13) and (6.14). Here we define

$$(7.7) \quad \epsilon_{\phi'} = \max_{\hat{x} \in I} \frac{\phi' - \rho_{\text{dis}}}{\rho_{\text{dis}}},$$

where  $\rho_{\text{dis}}$  denotes the density computed by the DDD simulations;  $I = [0.1, 1]$  where the boundary image effect disappears.  $\epsilon_{\phi'}$  measures the relative difference between the pair density coming from the two models. In a similar sense, we also define the relative difference in pair width

$$(7.8) \quad \epsilon_{\zeta} = \frac{\zeta - \zeta_{\text{dis}}}{\zeta_{\text{dis}}}.$$

In Table. 1,  $\epsilon_{\phi'}$  and  $\epsilon_{\zeta}$  at various time slots are shown. It is seen that the difference

$\hat{t}$	1	2	5	10	20	26.4
$\epsilon_{\phi'}$	0.0219	0.0195	0.0115	0.0088	0.0135	0.0139
$\epsilon_{\zeta}$	0.0805	0.0809	0.0811	0.0812	0.0814	0.0814

TABLE 1

$\epsilon_{\phi'}$  measures the relative difference between the pair density coming from the DDD and continuum models at various time slots and so does  $\epsilon_{\zeta}$  in pair width. Here  $S = 0.3$ ,  $\hat{\tau}_{\text{ext}}^0 = 0.5$ ,  $\partial\hat{\tau}_{\text{ext}}^0/\partial\hat{y} = 1$  and  $N = 50$ .

in pair density is no more than 2%, while the difference in pair width is roughly 10%.

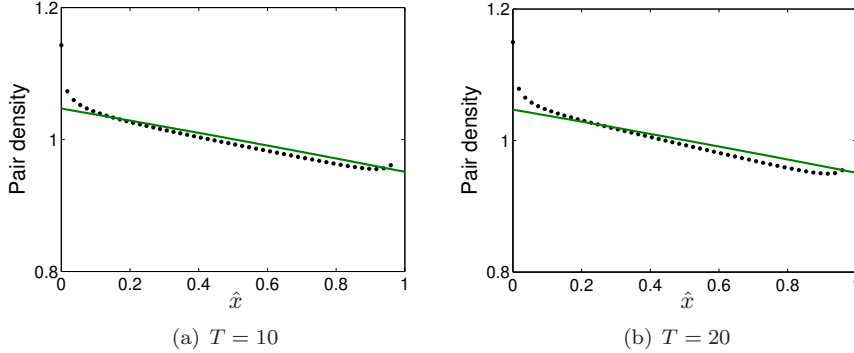


FIG. 14. Snap shots of pair density by DDD and the continuum methods at  $\hat{t} = 10$  and  $\hat{t} = 20$ .

In Fig. 14, snap shots of pair density by DDD and the continuum methods at  $\hat{t} = 10$  and  $\hat{t} = 20$  are shown.

The second set of numerical results are obtained by keeping all other parameters unchanged but increasing the total number  $N$ . It is worth noting that  $N$  has been scaled off in the derived continuum model. Hence an increase in  $N$  only affects the outcomes of the DDD models. In table 2, we list the comparison results between the two models with  $N$  varying. Here  $T_{\text{con}}$  and  $T_{\text{dis}}$  denote the actual time it takes to carry

$N$	50	100	150	200	500
$T_{\text{con}}/T_{\text{dis}}$	39.6447	4.9205	1.2298	0.5004	0.0220
$\epsilon_{\phi'}$	0.0132	0.0119	0.0112	0.0107	0.0092
$\epsilon_{\zeta}$	0.0814	0.0394	0.0257	0.0190	0.0072

TABLE 2

Comparison results by the derived continuum model and the DDD model with  $N$  varying. Here  $T_{\text{con}}$  and  $T_{\text{dis}}$  denote the real time it takes to carry out the simulation to steady states by the continuum and DDD model, respectively.  $T_{\text{con}}/T_{\text{dis}}$  measures to the computational efficiency of using the continuum model against its corresponding DDD model.

out the simulation to steady states by the continuum and DDD model, respectively.  $T_{\text{con}}/T_{\text{dis}}$  thus measures the computational efficiency of using the continuum model against its corresponding DDD model. As shown in Fig. 15(a),  $T_{\text{con}}/T_{\text{dis}}$  scales with  $N$  at an exponent of  $-3.25$ . The rationalisation of this number is as follows. For DDD simulation, the order to compute the pair-interaction among  $2N$  particles at each step takes time of  $\mathcal{O}(N^2)$ . This along with  $\mathcal{O}(N)$  steps needed to reach the equilibrium states (estimated with reference to Eq. (7.2)) adds up to computational time at  $\mathcal{O}(N^3)$ . On the other hand, the simulation at the continuum level stays the same for all  $N$ . It is these two factors that give rise to an exponent of almost  $-3$ .

To check the upscaling accuracy of our derived model, the differences in pair density and pair width against  $N$  are also listed in Table 2. It can be seen that both  $\epsilon_{\phi'}$  and  $\epsilon_{\zeta}$  drop with an  $N$  increasing as shown in Fig. 15(b). The observation meets our expectation, since the continuum model is obtained by performing asymptotic analysis in terms of  $1/N$ . An increased  $N$  effectively brings down the truncation error.

Moreover, the dynamical processes from the two models are also compared for the case when  $S$  is as small as 0.1. In this case, the governing equations at the continuum

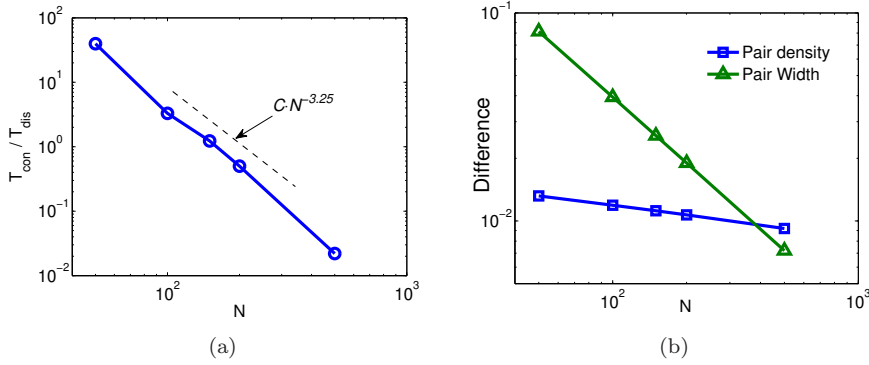


FIG. 15. (a)  $T_{con}/T_{dis}$  thus provides a measurement to the computational efficiency by the two models. The smaller this value is, the more efficient the continuum model is. (b) Differences in quantities of interest by using the derived continuum and DDD model.

level become Eq. (6.10), (6.15) and (6.16). In Table 3, the relative errors in the two quantities of interest are found no more than 10%. Provided the simple forms

$\hat{t}$	5	10	20	50	100	250
$\epsilon_{\phi'}$	0.0245	0.0340	0.0494	0.0603	0.0135	0.0120
$\epsilon_{\zeta}$	0.0469	0.0489	0.0522	0.0584	0.0814	0.0660

TABLE 3

Difference in the values  $\phi'$  and  $\zeta$  by the DDD and continuum models at various evolving time slot. Here  $S = 0.1$ ,  $\tau^0 = 0.5$ ,  $\partial\tau^0/\partial\hat{y} = 1$ ,  $N = 50$ .

displayed by the governing equations in this case, 10% deviation sounds acceptable.

From the comparison results presented above, the derived continuum model provides a good summary of the DDD model governed by Eq. (3.1) to (3.4) concerning the computational time saved and errors controlled under an acceptable level.

## 8. Conclusion and further discussion.

**8.1. Conclusion.** In this paper, we have studied the collective behaviour of a row of dislocation dipoles. The conclusion drawn from the analysis is summarised as follows.

It is found that the dislocation dipoles “pile-up” against an externally applied stress gradient. In another word, the dislocation pairs should be uniformly distributed in the absence of applied stress gradients.

When the externally applied stress is almost zero, we find three possible equilibrium patterns (as shown in Fig. 4), whose stability depends on the value of  $\phi'S$ , the ratio of the slip plane gap to the pair center spacing. If  $\phi'S$  is big (condition (5.13) breaks down), the non-localised structure (Equilibrium Type II) is the stable configuration. While  $\phi'S$  falls below the critical value 0.2465, a localised equilibrium structure (Equilibrium Type III) emerges. In this scenario, Equilibrium Type II is unstable and a natural transition to Equilibrium Type III is observed.

If the externally applied shear stress  $\tau_{ext}^0$  is non-negligible, the dislocation pair structures may break down provided that  $\tau_{ext}^0$  exceeds some critical value depending on  $S$ , the (rescaled) slip plane spacing. Two possible equilibrium patterns are found and the one with larger pair width gives rise to the stable configuration as suggested

by the shaded region in Fig. 6. The critical value of  $\tau_{\text{ext}}^0$  to break the dipole pairs is related to the strength of the matrix crystals.

The dynamics, if observed at the continuum level, can be viewed as two parallel processes taking place at different time scales. At the faster scale, the dislocation pairs rearrange themselves to satisfy the leading-order force balance equations. At the slower scale, the pair density evolves to equilibrium states, when the next order force balance equations are satisfied.

**8.2. Implication to the formation of PSBs.** The transition in equilibrium patterns from Type II to Type III, as suggested by our analysis, may shed light on the understanding of the formation of localised persistent slip band structures, which are found emerging among non-localised channel-vein structures. Practically, the transition in equilibrium patterns due to instability found in this paper may not be the only reason for the formation of PSBs, because the PSB walls consist more likely of several dislocation pairs rather than a single pair as indicated by the Equilibrium Type III. To further investigate the problem, one may also study the instability of the pair density equation (6.10). Another direction enlightened by our analysis is to further study the role of the externally applied stress gradient, which accounts for any non-uniformly distributed patterns according to our analysis.

**8.3. Implication to the incorporation of SSDs into existing continuum plasticity models.** As mentioned in the beginning of this paper, searching for a proper way to incorporate the statistically stored dislocations (SSDs) is one of the most challenging topics in the development of a dislocation-density-based model of plasticity, which is consistent with its underlying discrete dislocation dynamics. The analysis in this paper, however, may provide a way to clear the barricades posed by SSDs. Given  $\hat{t}$  the time scale associated with the continuum model (termed as the continuum time scale), it has been shown that the mutual adjustment within dislocation pairs characterised by  $\zeta$  varies so fast that only the steady (equilibrium) states are observable at the continuum time scale. On the other hand, the evolution of the pair density potential  $\phi$  takes place so slowly that it appears static observed at the continuum time scale.

Therefore, the information about the SSDs that should be maintained in the continuum model after the discrete-to-continuum transition, is the local equilibrium patterns of SSDs. In analogy with the case studied in this paper, the resulting continuum model is expected to be hierarchic. It should consist of a set of evolutionary equations for the geometrically necessary dislocations (GNDs) changing at a normal speed accompanied by another set of static equations describing the SSD structures in equilibrium, and the critical stress to break an SSD structure contributes to the crystal strength at the macroscopic level.

#### REFERENCES

- [1] M. ABRAMOWITZ AND I. A. STEGUN, eds., *Handbook of Mathematical Functions*, Dover Publications, Inc., New York, 10th ed., 1972.
- [2] A. ACHARYA, *A model of crystal plasticity based on the theory of continuously distributed dislocations*, J. Mech. Phys. Solids, 49 (2001), pp. 761–784.
- [3] S. BRINCKMANN AND E. VAN DER GIESSEN, *A discrete dislocation dynamics study aiming at understanding fatigue crack initiation*, Materials Science and Engineering a-Structural Materials Properties Microstructure and Processing, 387 (2004), pp. 461–464.

- [4] D. DICKEL, K. SCHULZ, S. SCHMITT, AND P. GUMBSCH, *Dipole formation and yielding in a two-dimensional continuum dislocation model*, Physical Review B, 90 (2014), p. 094118. PRB.
- [5] A. EL-AZAB, *Statistical mechanics treatment of the evolution of dislocation distributions in single crystals*, Physical Review B, 61 (2000), pp. 11956–11966.
- [6] M. G. D. GEERS, R. H. J. PEERLINGS, M. A. PELETIER, AND L. SCARDIA, *Asymptotic behaviour of a pile-up of infinite walls of edge dislocations*, Archive for Rational Mechanics and Analysis, 209 (2013), pp. 495–539.
- [7] I. GROMA, *Link between the microscopic and mesoscopic length-scale description of the collective behavior of dislocations*, Physical Review B, 56 (1997), pp. 5807–5813.
- [8] I. GROMA, F. F. CSIKOR, AND M. ZAISER, *Spatial correlations and higher-order gradient terms in a continuum description of dislocation dynamics*, Acta Mater., 51 (2003), pp. 1271–1281.
- [9] C. L. HALL, S. J. CHAPMAN, AND J. R. OCKENDON, *Asymptotic analysis of a system of algebraic equations arising in dislocation theory*, Siam Journal on Applied Mathematics, 70 (2010), pp. 2729–2749.
- [10] A. K. HEAD, S. D. HOWISON, J. R. OCKENDON, AND S. P. TIGHE, *An equilibrium-theory of dislocation continua*, Siam Review, 35 (1993), pp. 580–609.
- [11] J. P. HIRTH AND J. LOTHE, *Theory of dislocations*, Wiley, New York, 2nd ed., 1982.
- [12] T. HOCHRAINER, S. SANDFELD, M. ZAISER, AND P. GUMBSCH, *Continuum dislocation dynamics: Towards a physical theory of crystal plasticity*, J. Mech. Phys. Solids, 63 (2014), pp. 167–178.
- [13] H. MUGHRABI, *Microscopic mechanisms of metal fatigue*, in Proc. 5th Int. Conf. on the Strength of Metals and Alloys, vol. 3, Pergamon, Oxford, 1980, p. 1615.
- [14] H. OCKENDON AND J. R. OCKENDON, *Dynamic dislocation pile-ups*, Philosophical Magazine a-Physics of Condensed Matter Structure Defects and Mechanical Properties, 47 (1983), pp. 707–719.
- [15] R. E. VOSKOBOINIKOV, S. J. CHAPMAN, J. R. OCKENDON, AND D. J. ALLWRIGHT, *Continuum and discrete models of dislocation pile-ups. i. pile-up at a lock*, J. Mech. Phys. Solids, 55 (2007), pp. 2007–2025.
- [16] Y. XIANG, *Continuum approximation of the peach-coehler force on dislocations in a slip plane*, J. Mech. Phys. Solids, 57 (2009), pp. 728–743.
- [17] X. H. ZHU AND Y. XIANG, *Continuum model for dislocation dynamics in a slip plane*, Philosophical Magazine, 90 (2010), pp. 4409–4428.
- [18] X. H. ZHU AND Y. XIANG, *Continuum framework for dislocation structure, energy and dynamics of dislocation arrays and low angle grain boundaries*, J. Mech. Phys. Solids, 69 (2014), pp. 175–194.
- [19] Y. C. ZHU AND S. J. CHAPMAN, *A natural transition between equilibrium patterns of dislocation dipoles*, J. Elast., 117 (2014), pp. 51–61.
- [20] Y. C. ZHU, H. Q. WANG, X. H. ZHU, AND Y. XIANG, *A continuum model for dislocation dynamics incorporating frank-read sources and hall-petch relation in two dimensions*, Int. J. Plast., 60 (2014), pp. 19–39.
- [21] Y. C. ZHU AND Y. XIANG, *A continuum model for dislocation dynamics in three dimensions using the dislocation density potential functions and its application in understanding the micro-pillar size effect*, Submitted for publication.